

Solution Structure of Recombinant Hirudin and the Lys-47 → Glu Mutant: A Nuclear Magnetic Resonance and Hybrid Distance Geometry-Dynamical Simulated Annealing Study[†]

Paul J. M. Folkers,^{‡§} G. Marius Clore,^{*‡} Paul C. Driscoll,[‡] Johannes Dodt,^{||} Stefanie Köhler,^{||} and Angela M. Gronenborn^{*‡}

Laboratory of Chemical Physics, National Institute of Diabetes and Digestive and Kidney Diseases, National Institutes of Health, Bethesda, Maryland 20892, and Institut für Biochemie, Technische Hochschule Darmstadt, Petersenstrasse 22, D-6100 Darmstadt, West Germany

Received August 15, 1988; Revised Manuscript Received October 18, 1988

ABSTRACT: The solution structure of recombinant wild-type hirudin and of the putative active site mutant Lys-47 → Glu has been investigated by nuclear magnetic resonance (NMR) spectroscopy at 600 MHz. The ¹H NMR spectra of the two hirudin variants are assigned in a sequential manner with a combination of two-dimensional NMR techniques. Some assignments made in our previous paper [Sukumaran, D. K., Clore, G. M., Preuss, A., Zarbock, J., & Gronenborn, A. M. (1987) *Biochemistry* 26, 333-338] were found to be incorrect and are now corrected. Analysis of the NOE data indicates that hirudin consists of an N-terminal compact domain (residues 1-49) held together by three disulfide linkages and a disordered C-terminal tail (residues 50-65) which does not fold back on the rest of the protein. This last observation corrects conclusions drawn by us previously on hirudin extracted from its natural source, the leech *Hirudo medicinalis*. The improved sensitivity of the 600-MHz spectrometer relative to that of our old 500-MHz spectrometer, the availability of two variants with slightly different chemical shifts, and the additional information arising from stereospecific assignments of methylene β-protons and methyl protons of valine have permitted the determination of the solution structure of hirudin with much greater precision than before. Structure calculations on the N-terminal domain using the hybrid distance geometry-dynamical simulated annealing method were based on 685 and 661 approximate interproton distance restraints derived from nuclear Overhauser enhancement (NOE) data for the wild-type and mutant hirudin, respectively, together with 16 distance restraints for 8 backbone hydrogen bonds identified on the basis of NOE and amide NH exchange data and 26 ϕ backbone and 18 χ₁ side-chain torsion angle restraints derived from NOE and three-bond coupling constant data. A total of 32 structures were computed for both the wild-type and mutant hirudin. The structure of residues 2-30 and 37-48 which form the core of the N-terminal domain is well determined in both cases with an average atomic rms difference between the individual structures and the respective mean structures of ~0.7 Å for the backbone atoms and ~1 Å for all atoms. As found previously, the orientation of the exposed finger of antiparallel β-sheet (residues 31-36) with respect to the core could not be determined on the basis of the present data due to the absence of any long-range NOEs between the exposed finger and the core. The Lys-47 → Glu mutation has only a small, but clearly discernible, effect on the structure which can be attributed to the larger space requirement for the longer Lys side chain relative to that of the shorter Glu side chain.

Hirudin, a small protein of 65 residues from the leech *Hirudo medicinalis*, is the most potent natural inhibitor of coagulation known (Haycraft, 1884; Markwardt, 1970). Hirudin acts by binding specifically and very tightly ($K_{\text{assoc}} \sim 10^{12}$ - 10^{14} M⁻¹) to α-thrombin (Stone et al., 1986; Dodt et al., 1988), thereby abolishing its ability to cleave fibrinogen (Magnusson, 1972; Markwardt 1985). In animal systems the antithrombotic effect of hirudin is most effective in stasis-induced venous thrombosis and in disseminated intravascular coagulation (Markwardt et al., 1988). These pharmacological properties, together with its apparent lack of antigenicity and toxicity, have prompted considerable interest with regard to its potential clinical use (Nowak & Markwardt, 1980; Ishikawa et al., 1980; Walsmann & Markwardt, 1981; Markwardt et al., 1982, 1988; Kloss & Mittman, 1982).

Recently, overexpression of the structural gene of hirudin in *Escherichia coli* has been achieved for several hirudin variants (Harvey et al., 1986; Bergmann et al., 1986; Dodt et al., 1986; Fortkamp et al., 1986), thereby making available large quantities of highly purified hirudin for structural and functional studies. Unlike natural hirudin isolated from the leech, Tyr-63 is not sulfated in the recombinant hirudins. This, however, has only a minor effect on the binding to thrombin (Dodt et al., 1988). Kinetic and equilibrium measurements have shown that a single hirudin molecule occupies at least two sites on α-thrombin simultaneously, one of which is the catalytic site, and that at least one binding site distinct from the catalytic site is important in the binding of hirudin to α-thrombin (Fenton et al., 1979; Fenton, 1981; Chang, 1983; Stone & Hofsteenge, 1986; Stone et al., 1987; Krstenansky & Mao, 1987). Studies with synthetic peptides have shown that the interaction with the latter site involves the C-terminal residues 54-65 (Owen et al., 1988). Sequence comparison (Petersen et al., 1976) with the region in prothrombin (residues 148-156) containing the site (Arg-155-Ser-156) at which prothrombin undergoes self-cleavage to generate thrombin

[†]This work was supported by the Intramural AIDS Targeted Antiviral Program of the Office of the Director, NIH (G.M.C. and A.M.G.).

[‡]National Institutes of Health.

[§]P.J.M.F. was supported in part by the Foundation for Advanced Education in the Sciences at the National Institutes of Health.

^{||}Technische Hochschule Darmstadt.

indicates a 50% homology with residues 40–48 of hirudin, suggesting that Lys-47 may be the P1 residue (notation of Schechter & Berger, 1967) which binds to the primary specificity pocket of thrombin. To test this hypothesis, site-specific mutagenesis has been carried out, altering in turn the four basic residues of hirudin, Lys-27, Lys-36, Lys-47, and His-51 (Dodt et al., 1988). Only mutations at position 47 had an effect on the stability of the hirudin–thrombin complex. The Lys-47 → Glu mutant had the most significant effect with a 10-fold reduction in the equilibrium association constant which could be attributed entirely to an increase in the dissociation rate constant. These data imply that while the hirudin–thrombin recognition process is independent of the nature of the putative reactive site, the stability of the complex is positively influenced by Lys-47 which may bind to the primary specificity pocket of thrombin, thereby inhibiting the hydrolysis of smaller substrates (Dodt et al., 1988).

Previously, we presented the ^1H nuclear magnetic resonance (NMR)¹ assignments and determination of the secondary structure of natural hirudin isolated and purified from the whole body of leeches (Sukumaran et al., 1987). In addition, the approximate polypeptide fold was determined on the basis of NOE-derived interproton distances from metric matrix distance geometry and restrained molecular dynamics calculations (Clore et al., 1987a). The structures had two ill-defined regions comprising residues 31–36 and 58–65 and a better defined central core (residues 3–30, 37–46, and 56–57). The backbone atomic rms difference between the individual calculated structures and the mean structure for the core residues was still ~ 2 Å, which is considerably worse than that which can be achieved by X-ray crystallography. Further, the conformations of the majority of the side chains, with a few exceptions, were not well defined. It was therefore clear that a more precise definition of the structure of hirudin would be an essential prerequisite for attempting to understand the mechanism of its inhibition of thrombin. To pursue this goal, we set out to extract a larger number of structural restraints from the NMR data using the newly available recombinant wild-type and mutant proteins. In this respect, stereospecific assignments of methylene proton resonances, as well as the increased stability, sensitivity, line shape, and resolution offered by our present 600-MHz spectrometer relative to those of our old 500-MHz spectrometer, were important contributory factors in enabling us to obtain a significantly larger number of interproton distances.

In this paper, we present an investigation into the solution structure of recombinant wild-type hirudin and of the Lys-47 → Glu mutant. Both hirudin spectra are completely assigned with a number of two-dimensional NMR techniques. During the course of this work we found that some assignments made in our previous paper were incorrect (Sukumaran et al., 1987). One clear consequence of this is that *no* evidence could now be found for any interaction between the C-terminal tail and the core of the protein, leading to the conclusion that the C-terminal region extending from residue 50 to residue 65 is disordered. Structure calculations were therefore carried out only for residues 1–49. These were based on 758 and 737 experimental restraints for the wild-type and mutant hirudin, respectively, of which $\sim 92\%$ comprised approximate inter-

proton distance restraints, the remainder being made up of hydrogen-bond, ϕ backbone torsion angle, and χ_1 side-chain torsion angle restraints. This represents about 2.5 times the number of experimental restraints used to calculate the structure of natural wild-type hirudin previously (Clore et al., 1987a). Thirty-two structures were computed for both proteins with the hybrid distance geometry–dynamical simulated annealing method (Nilges et al., 1988a). The core of the molecule is formed by residues 2–30 and 37–48, and the average atomic rms difference between the core of the individual structures and the mean structure obtained by averaging their coordinates is ~ 0.7 Å for the backbone atoms and ~ 1 Å for all atoms. The polypeptide fold of the core is similar to that determined previously (Clore et al., 1987a) with the one difference that the twist and orientation of the segment extending from residue 18 to residue 25 are altered. Further, the conformations of a number of side chains are uniquely defined. A comparison of the two sets of structures enables one to identify, within the precision of the NMR method, small differences between the wild-type and mutant hirudin structures.

EXPERIMENTAL PROCEDURES

Sample. The gene for hirudin was synthesized chemically and expressed in *E. coli* under control of the tac promoter (Dodt et al., 1986). The Lys-47 → Glu variant was generated by oligonucleotide-directed mutagenesis (Dodt et al., 1988). Wild-type and mutant hirudin were isolated from the periplasmic fractions of *E. coli* (Chan et al., 1981) as described previously (Dodt et al., 1986). Purity was ascertained by high-pressure liquid chromatography and amino acid sequencing. Both NMR samples contained 5 mM hirudin in either 90% $\text{H}_2\text{O}/10\%$ D_2O or 99.996% D_2O , pH 3.0.

NMR Spectroscopy. NMR spectra were recorded on a Bruker AM 600 spectrometer equipped with digital phase shifters, a “reverse”-mode ^1H probe, and an Aspect 3000 computer. All two-dimensional spectra were recorded in the pure-phase absorption mode according to the time proportional incrementation method (Redfield & Kuntz, 1975) as described by Marion and Wüthrich (1983). A complete set of spectra was recorded at 27 °C in both H_2O and D_2O , and some additional spectra were recorded at 19 °C. HOHAHA (Braunschweiler & Ernst, 1983; Davis & Bax, 1985) spectra were recorded with mixing times of approximately 50 ms. The radio-frequency pulses in the HOHAHA experiments were generated via the high-power decoupler channel (90° pulse ~ 25 – 27 μs), and anisotropic mixing was carried out with the WALTZ-17_y pulse scheme sandwiched between 1.5-ms trim pulses (Bax, 1988). NOESY (Jeener et al., 1979) spectra were recorded at mixing times ranging from 50–200 ms. At the shorter mixing times zero quantum effects were suppressed by use of either a 5% random variation of the mixing time (Macura et al., 1981) or a systematic approach similar to that described by Rance et al. (1985). For measurements in H_2O , the water resonance was suppressed by a semiselective excitation pulse sequence. In the case of NOESY spectra this involved replacing the last 90° pulse in the sequence by the jump-return sequence (90°_x– τ –90°_{-x}) with the carrier placed at the position of the solvent resonance (Plateau & Guéron, 1982). Typically, a τ value of 90 μs was chosen. In the case of the HOHAHA spectra the mixing sequence was followed by a sequence consisting of a 90° “flipback” pulse, a recovery delay (100 μs), and the jump-return sequence (Bax et al., 1987). In addition, the unwanted effects of radiation damping were avoided by shifting the phase of the preparation pulse 45° out of register with those of the evolution and detection

¹ Abbreviations: NMR, nuclear magnetic resonance; NOE, nuclear Overhauser effect; NOESY, two-dimensional NOE spectroscopy; COSY, homonuclear two-dimensional correlated spectroscopy; E-COSY, exclusive two-dimensional correlated spectroscopy; HOHAHA, two-dimensional homonuclear Hartmann-Hahn spectroscopy; FID, free induction decay; rms, root mean square; SA, simulated annealing.

periods (Bax, Clore, Driscoll, and Gronenborn, unpublished data). Optimization of the receiver phase was performed to eliminate base-line distortions (Marion & Bax, 1988). Furthermore, in the case of a strong solvent signal, the first point of each FID was set to zero, and a linear base-line correction was applied to both the initial FIDs and the F2 cross sections prior to Fourier transformation in F1. This suppresses undesirable t_2 ridges arising from the large solvent resonance and improves significantly the line-shape appearance of the residual water signal. Typically, 800–1024 increments of 2K data points were recorded with 8–32 transients each, yielding, after zero filling, spectra with a digital resolution ranging from 6.2 to 8.0 Hz per point. The relaxation delays used were between 1.6 and 2 s.

COSY (Aue et al., 1976) spectra were also recorded in H₂O with 4K data points by presaturation of the solvent resonance. For analysis zero filling was employed to increase the digital resolution to 0.8 Hz per point in F2 and 6.4 Hz per point in F1.

E-COSY spectra were recorded in D₂O to measure $^3J_{\alpha\beta}$ coupling constants as well as to unambiguously identify direct correlations in the HOHAHA spectra. A total of 1024 increments of 4K data points were recorded with a 64-step phase cycle (Griesinger et al., 1985, 1987). After zero filling, spectra were obtained with a digital resolution of 0.78 Hz per point in F2 and 3.13 Hz per point in F1.

The present study was aided by the superior performance of our Bruker AM600 600-MHz spectrometer relative to that of our old Bruker AM500 500-MHz spectrometer. In this respect some quantitative comparison of these two spectrometers is useful. The signal-to-noise ratios of the our 600-MHz and 500-MHz spectrometers are 750:1 and 280:1, respectively, for a sample of 0.1% ethylbenzene (ASTM standard). The nonspinning line shape for a sample of 3% chloroform (ASTM standard) is 8 and 16 Hz at 0.55% and 0.11% peak height on the 600-MHz spectrometer compared to 24 and 50 Hz, respectively, on the 500-MHz spectrometer. This made sample spinning on the 500-MHz spectrometer essential to improve the line width to values of 10 and 20 Hz at 0.55% and 0.11% peak height, respectively. As a result, additional t_1 noise arising from spinning was invariably present in the old 500-MHz spectra. In contrast, all 2D experiments on the 600-MHz spectrometer were conducted nonspinning. The stability of the spectrometer as measured by peak to peak difference for two consecutive transients is significantly greater for the 600-MHz spectrometer: measured relative to the sum of the two successive signals, the maximum difference for the 600-MHz spectrometer is <0.5% nonspinning, compared to 5% for the 500-MHz spectrometer spinning. (Note the value for the 500-MHz spectrometer nonspinning is irrelevant as all 2D experiments on that machine had to be performed with the sample spinning due to the line-shape factors discussed above.) Finally, the resolution of a 2D spectrum increases as the square of the field, resulting in a 44% increase in resolution on going from 500 to 600 MHz.

Calculations. Three-dimensional structures were calculated on the basis of the NMR data with the hybrid metric matrix distance geometry–dynamical simulated annealing approach (Nilges et al., 1988a). The metric matrix distance geometry calculations (Crippen & Havel, 1978; Kuntz et al., 1979; Havel et al., 1983) were carried out with the program DISGEO (Havel & Wüthrich, 1985; Havel, 1986). The dynamical simulated annealing calculations were carried out with the program XPLOR (Brünger, unpublished data; Brünger et al., 1986, 1987a,b). XPLOR was derived originally from the program

CHARMM (Brooks et al., 1983) and has been especially adapted for restrained molecular dynamics (Clore et al., 1985; Brünger et al., 1986) and dynamical simulated annealing (Nilges et al., 1988a,b,c). All computations were carried out on either Micro VaxII or VAX 8530 computers. Structures were displayed with a modified version of the function network of FRODO (Jones, 1978) interfaced with XPLOR on an Evans & Sutherland PS390 color graphics system.

The details of the hybrid distance geometry–dynamical simulated annealing approach have been described previously (Nilges et al., 1988a) and will only be briefly summarized here. The calculations are divided into two stages.

In the first stage, a set of distance values between a subset of atoms (comprising the N, C, C α , C α H, C β , nonterminal C γ and C δ atoms, and a pseudoatom for the aromatic ring of Tyr and Phe) is generated at random within the distance bounds imposed by all the experimental restraints, the complete covalent geometry, and the hard-sphere atomic van der Waals radii. A substructure is then obtained by projection of the resulting distance matrix from n -dimensional distance space into Cartesian coordinate space. As the randomly chosen distances are not checked with respect to the triangle inequalities, this procedure takes only a small amount of computational time (~ 10 min on a VAX 8530 computer). Different substructures are produced by using different random number seeds to generate the initial distance matrix. The coordinates of the substructures are used as the starting points for the subsequent calculations. It should be noted that some of the substructures have a polypeptide fold that is a mirror image of the correct fold. These are easily identified as they have D- instead of L-amino acids.

The second stage involves the application of dynamical simulated annealing (Nilges et al., 1988a,b) in real Cartesian coordinate space, in which Newton's equations of motion are solved subject to a total target function which is made up of the following terms:

$$F_{\text{tot}} = F_{\text{covalent}} + F_{\text{repel}} + F_{\text{NOE}} + F_{\text{tor}} \quad (1)$$

and which represents in effect the potential energy of the system. Unlike the empirical energy function used in restrained energy minimization and molecular dynamics calculations in which the nonbonded interactions are represented by electrostatic, van der Waals, and hydrogen-bonding potentials (Kaptein et al., 1985; Clore et al., 1985, 1986a), the nonbonded interaction term in F_{tot} is given solely by a simple van der Waals repulsion term (F_{repel}).

F_{covalent} is the target function for maintaining correct bond lengths, angles, and planes and is given by

$$F_{\text{covalent}} = \sum_{\text{bonds}} k_b(r - r_0)^2 + \sum_{\text{angles}} k_\theta(\theta - \theta_0)^2 + \sum_{\text{impropers}} k_\omega(\omega - \omega_0)^2 \quad (2)$$

The values chosen for the force constants for the bond (k_b), angle (k_θ), and improper torsions (k_ω) are set to uniform high values to ensure near perfect stereochemistry throughout the calculations, namely, 600 kcal·mol⁻¹·Å⁻², 500 kcal·mol⁻¹·rad⁻², and 500 kcal·mol⁻¹·rad⁻², respectively. (Note that the improper torsions serve to maintain planarity and chirality, and the conformation about the peptide bonds is assumed to be planar and trans.)

F_{repel} is the target function used to prevent unduly close nonbonded contacts and is given by

$$F_{\text{repel}} = \begin{cases} 0 & \text{if } r \geq sr_{\text{min}} \\ k_{\text{vdw}}(s^2r_{\text{min}}^2 - r^2)^2 & \text{if } r < sr_{\text{min}} \end{cases} \quad (3)$$

The values of r_{min} are the standard values of the van der Waals

radii as represented by the Lennard–Jones van der Waals radii used in the CHARMM empirical energy function (Brooks et al., 1983). The van der Waals radius scale factor s is set to 0.8 in the present calculations, and the resulting hard sphere van der Waals radii are similar to those used in various other distance geometry programs (Havel, 1986; Braun & Go, 1985; Billeter et al., 1987).

F_{NOE} and F_{tor} are the target functions for the NOE and torsion angle restraints and are represented by square-well potentials of the form (Clare et al., 1986b)

$$F_{\text{NOE}} = \begin{cases} k_{\text{NOE}}(r_{ij} - r_{ij}^u)^2 & \text{if } r_{ij} > r_{ij}^u \\ 0 & \text{if } r_{ij}^l \leq r_{ij} \leq r_{ij}^u \\ k_{\text{NOE}}(r_{ij} - r_{ij}^l)^2 & \text{if } r_{ij} < r_{ij}^l \end{cases} \quad (4)$$

and

$$F_{\text{tor}} = \begin{cases} k_{\text{tor}}(\varphi_i - \varphi_i^u)^2 & \text{if } \varphi_i > \varphi_i^u \\ 0 & \text{if } \varphi_i^l \leq \varphi_i \leq \varphi_i^u \\ k_{\text{tor}}(\varphi_i - \varphi_i^l)^2 & \text{if } \varphi_i < \varphi_i^l \end{cases} \quad (5)$$

where k_{NOE} and k_{tor} are variable force constants, r_{ij}^u and φ_i^u are the upper limits for the distance and torsion angle restraints, respectively, and r_{ij}^l and φ_i^l are the corresponding lower limits.

The starting coordinates for the dynamical simulated annealing calculations are obtained by best fitting one residue at a time to the subset of atoms present in the substructures and subjecting the resulting coordinates to 200 cycles of Powell minimization to regularize the peptide bond. The dynamical simulated annealing protocol involves three steps: (i) 3.75-ps dynamics at 1000 K during which time k_{NOE} and k_{tor} are increased from 1 to 50 kcal·mol⁻¹·Å⁻² and from 5 to 200 kcal·mol⁻¹·rad⁻², respectively, by doubling their values every 75 fs, k_{repel} is increased from 0.01 to 4.0 kcal·mol⁻¹·Å⁻⁴ by multiplying its values by 400^{1/150} every 75 fs, and the velocities are rescaled to 1000 K every 75 fs (the values of k_{NOE} , k_{tor} , and k_{repel} reached at the end of this step are maintained for the remainder of the calculation); (ii) 1.5-ps dynamics at 300 K rescaling the velocities to 300 K every 100 fs; (iii) 200 cycles of Powell minimization. In the case of hirudin₁₋₄₉ this protocol took ~2 h on a VAX 8530 (equivalent to ~1 h on a VAX 8550), and the average backbone atomic rms shifts produced by dynamical simulated annealing were ~2.5 Å for the backbone atoms and ~3.5 Å for all atoms.

As in previous studies (Nilges et al., 1988a,b; Driscoll et al., 1989), the dynamical simulated annealing structures are referred to as SA structures, the mean structure obtained by averaging their coordinates is referred to as $\overline{\text{SA}}$, and the structure obtained by restrained minimization of $\overline{\text{SA}}$ is referred to as $(\overline{\text{SA}})_r$. We note that the $(\overline{\text{SA}})_r$ structure is in general closer to the mean structure than any of the individual SA structures and, unlike the mean structure, has good stereochemistry and nonbonded contacts (Clare et al., 1986a).

RESULTS AND DISCUSSION

Assignment of the ¹H NMR Spectrum. The complete assignment of both recombinant hirudin spectra was performed according to well-established methods (Wüthrich et al., 1982; Wüthrich, 1986). This involves identification of through-bond scalar connectivities, followed by sequential resonance assignment using short through-space (<5 Å) NOE connectivities involving the NH, C^αH, and C^βH protons as well as the C^δH protons of proline. The through-bond connectivities were principally established by using the HOHAHA spectra, which demonstrate both direct and multiple relayed correlations. Unambiguous identification of direct scalar connectivities was achieved with reference to the COSY and E-COSY spectra

recorded in H₂O and D₂O, respectively. Examples of HOHAHA spectra in H₂O are shown in Figure 1. At a mixing time of 50 ms in H₂O, all the NH–C^αH correlations as well as many relayed connectivities are apparent. Examples of NOESY spectra in H₂O are shown in Figures 2 and 3. Additional spectra are included in the supplementary material (see paragraph at end of paper regarding supplementary material).

The availability of two samples exhibiting slightly different chemical shifts was of major advantage over our previous study (Sukumaran et al., 1987) in resolving ambiguities. This was further aided by the superior resolution, sensitivity, line shape, and stability afforded by our present 600-MHz spectrometer relative to those of our old 500-MHz spectrometer (see Experimental Procedures). As a result, some resonance assignments made previously (Sukumaran et al., 1987) were found to be incorrect, and these are documented below.

The spin systems of Phe-56 and Asn-12 were incorrectly assigned in the previous study. For both the natural and recombinant wild-type hirudins, the NH and C^αH resonances of these residues are degenerate. In the spectrum of the mutant protein, however, the amide NH signals are resolved sufficiently to identify the sequential $d_{\alpha\text{N}}(i,i+1)$ connection from Gln-11 and thus to correctly attach the C^βH₂ groups for residues 12 and 56. The assignment of Phe-56 is secured via intraresidue ring-to-backbone C^βH–C^βH NOEs and the assignment of Asn-12 via sequential $d_{\beta\text{N}}(i,i+1)$ NOEs to Gly-13 and intraresidue NH₂–C^βH NOEs (see Figure 2).

Further revisions of previous assignments all involved residues from, or to, which hardly any sequential NOEs were observed before. The use of the mutant revealed clear sequential NOEs connecting residues 4, 5, and 6, resulting in the reassignment of Asp-5 (Figure 2). This reassignment also accounted for a previously unassigned C^αH–C^βH cross-peak at 4.95/2.90 ppm appearing in the HOHAHA spectra of natural hirudin in D₂O. In the natural hirudin, the intraresidue NH–C^αH through-bond connectivity of Asp-5 at 500 MHz was absent. Furthermore, the NH position of this residue is almost identical with that of residues 4 and 6 in the wild-type hirudin (Figure 1A) which, in the absence of the mutant, would have made it very difficult to assign all three residues correctly. Other reassignments involve residues 53, 54, and 55 and the NH resonance position of Ser-9. As in the case of Asp-5, the NH(*i*)–C^αH(*i*) cross-peak for Ser-9 was not present in the 500-MHz spectra of natural hirudin.

The assignments of the C-terminal portion of the protein (residues 49–65) were revised in light of an extensive study of the recombinant proteins as well as a reexamination of the natural protein, involving evaluation of the effects of temperature of the spectrum. This was important as residues 55, 56, 57, and 59 possess virtually degenerate NH chemical shifts under all conditions studied. It is worth pointing out that all the reassignments involve residues which lie outside regions of regular secondary structure such that the chemical shift dispersion is much reduced. Further, with the benefit of hindsight, it is clear that some of the incorrect assignments were due to an overinterpretation of ambiguous connectivities.

The natural hirudin studied previously (Sukumaran et al., 1987) contained a small proportion, albeit ≤10%, of minor isoprotein variants with slightly altered sequences. In contrast, the recombinant proteins are homogeneous. In the present study, it became clear that some of the cross-peaks which were observed but not assigned in the previous study were also present in the spectra of the recombinant proteins. They must therefore correspond to some minor conformational form of

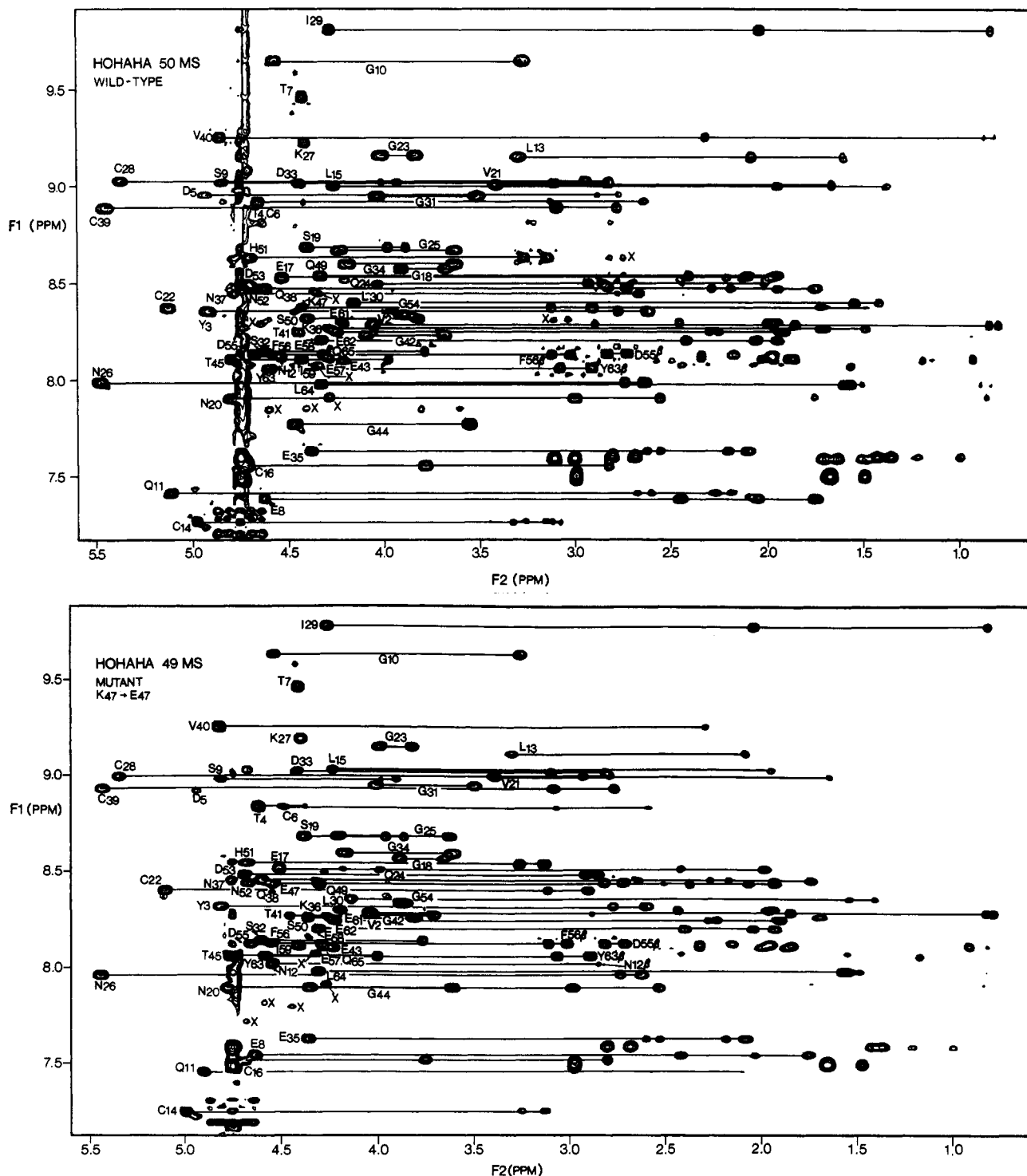


FIGURE 1: NH (F1 axis)-aliphatic (F2 axis) region of the HOHAHA spectrum of both recombinant wild-type and mutant hirudin in H_2O at 27 °C. Some relayed connectivities are indicated by continuous lines, and the labels are at the positions of the direct NH-C α H cross-peaks. All NH-C α H connectivities are visible in both spectra. Note that the NH-C α H cross-peaks of Thr-4 and Cys-6 overlap in the spectrum of the wild type. Peaks marked with an X are unassigned and arise from a minor conformational form of the protein (see text).

the protein. These peaks, as well as some additional minor peaks not observed previously, are labeled with an X in the HOHAHA spectra in H_2O shown in Figure 1. Clear examples of this phenomenon are also observed in the D_2O HOHAHA spectrum where an additional set of minor peaks with slightly different chemical shifts from the corresponding major peaks for Leu-13 and Val-21 are observed (see supplementary material). The structure of this minor conformational form could not be determined since it is of such low abundance that no meaningful NOEs could be observed for further structural interpretation.

A summary of the short-range NOEs involving the NH, C α H, and C β H protons, as well as the C δ H protons of proline, is shown in Figure 4. A complete list of assignments for both proteins is given in Table I. As the chemical shifts were measured to an accuracy of ± 0.01 ppm, only spin systems with chemical shifts which differ by 0.03 ppm or more from those of the wild type are listed for the mutant. Comparison of the chemical shifts of wild-type and mutant hirudin shows that the Lys-47 \rightarrow Glu mutation has a significant effect on the resonance positions of many amino acids, and these will be discussed later in light of the computed structures.

Table I: Proton Resonance Assignments of Hirudin at 27 °C and pH 3.0

residue	chemical shift (ppm)			
	NH	C $^{\alpha}$ H	C $^{\beta}$ H $^{\alpha}$	others b
(A) Wild-Type Hirudin				
V1		3.65	1.92	C $^{\gamma}$ H $_3$ 0.77, 0.63
V2	8.28	4.07	1.87	C $^{\gamma}$ H $_3$ 0.86, 0.81 $^+$
Y3	8.45	4.93	2.79,* 2.63	C $^{\delta}$ H 7.03; C $^{\epsilon}$ H 6.65
T4	8.92	4.67	4.43	C $^{\gamma}$ H 1.20
D5	8.95	4.95	2.90,* 2.78	
C6	8.92	4.65	3.14,* 2.65	
T7	9.46	4.43	4.43	C $^{\gamma}$ H $_3$ 1.23
E8	7.38	4.64	2.06, 1.77	C $^{\gamma}$ H 2.48, 2.45
S9	9.02	4.86	4.02,* 3.94	
G10	9.64	4.58, 3.29		
Q11	7.41	5.14	2.28, 2.20	C $^{\gamma}$ H 2.68, 2.61; NH $_2$ 7.74, 6.76
N12	8.11	4.55	3.00, 2.87	NH $_2$ 7.36, 6.09
L13	9.15	3.31	2.10, 2.10	C $^{\gamma}$ H 1.61; C $^{\delta}$ H $_3$ 0.98, 0.89
C14	7.27	4.99	3.34,* 3.11	
L15	9.00	4.28	1.96, 1.40	C $^{\gamma}$ H 1.21; C $^{\delta}$ H 0.81, 0.49
C16	7.56	4.72	3.80, 2.83	
E17	8.52	4.55	2.13, 2.01	C $^{\gamma}$ H 2.46, 2.23
G18	8.57	3.92, 3.68		
S19	8.68	4.41	3.99, 3.90*	
N20	7.90	4.81	3.01, 2.57*	NH $_2$ 7.43, 7.02
V21	9.00	3.43	1.68	C $^{\gamma}$ H 0.33,* 0.29
C22	8.37	5.14	2.92, 3.14*	
G23	9.16	4.01, 3.84		
Q24	8.49	4.05	2.03, 2.03	C $^{\gamma}$ H 2.44, 2.44; NH $_2$ 7.55, 6.93
G25	8.68	3.64, 4.25		
N26	7.99	5.49	2.75, 2.65	NH $_2$ 6.74, 6.11
K27	9.23	4.43	1.25, 1.25	C $^{\gamma}$ H 1.53, 1.00; C $^{\delta}$ H 1.44, 1.36 C $^{\epsilon}$ H 2.81, 2.69; N $^{\delta}$ H 7.60
C28	9.02	5.39	2.96, 2.84	
I29	9.80	4.30	2.06	C $^{\gamma}$ H 1.50, 1.39; C $^{\gamma}$ H $_3$ 0.85; C $^{\delta}$ H $_3$ 0.75
L30	8.40	4.16	1.56, 1.56	C $^{\gamma}$ H 1.43; C $^{\delta}$ H $_3$ 0.60, 0.60
G31	8.95	4.05, 3.53		
S32	8.15	4.63	3.80, 3.80	
D33	9.01	4.45	3.13, 2.84	
G34	8.60	4.19, 3.63		
E35	7.62	4.39	2.21,* 2.12	C $^{\gamma}$ H 2.63, 2.56
K36	8.26	4.30	1.74, 1.71	C $^{\gamma}$ H 1.99, 1.50; C $^{\delta}$ H 1.70, 1.74; C $^{\epsilon}$ H 3.21, 3.01; N $^{\delta}$ H 7.50
N37	8.44	4.79	2.67, 2.67	
Q38	8.47	4.63	1.97, 1.77	C $^{\gamma}$ H 2.30, 2.21
C39	8.89	5.46	3.11, 2.79*	
V40	9.25	4.87	2.34	C $^{\gamma}$ H $_3$ 0.89, 0.84 $^+$
T41	8.24	4.46	4.06	C $^{\gamma}$ H $_3$ 1.28
G42	8.23	4.10, 3.68		
E43	8.09	4.22	1.98, 1.98	C $^{\gamma}$ H 2.60, 2.51
G44	7.77	4.48, 3.55		
T45	8.10	4.81	3.98	C $^{\gamma}$ H $_3$ 1.22
P46		4.63	2.23, 1.90	C $^{\gamma}$ H 2.08; C $^{\gamma}$ H 3.92, 3.76
K47	8.37	4.44	1.73, 1.68	C $^{\gamma}$ H 1.50; C $^{\delta}$ H 1.72, 1.65; C $^{\epsilon}$ H 3.01, 3.13; N $^{\delta}$ H 7.59
P48		4.45	2.33, 1.90	C $^{\gamma}$ H 2.05, 2.01; C $^{\delta}$ H 3.99, 3.61
Q49	8.54	4.35	2.10, 1.97	C $^{\gamma}$ H 2.42, 2.42; NH $_2$ 7.62, 6.86
S50	8.32	4.41	3.85, 3.82	
H51	8.63	4.72	3.28, 3.16	C $^{\delta 2}$ H 7.29; C $^{\epsilon 1}$ H 8.61
N52	8.47	4.70	3.83, 2.75	
D53	8.50	4.72	2.94, 2.88	
G54	8.33	3.90		
D55	8.13	4.70	2.84, 2.74	
F56	8.13	4.58	3.13, 3.04	C $^{\delta}$ H 7.22; C $^{\epsilon}$ H 7.35; C $^{\epsilon}$ H 7.31
E57	8.10	4.30	2.02, 1.90	C $^{\gamma}$ H 2.35, 2.35
E58	8.20	4.34	2.07, 1.96	C $^{\gamma}$ H 2.43, 2.43
I59	8.11	4.44	1.89	C $^{\gamma}$ H 1.50, 1.15; C $^{\gamma}$ H $_3$ 0.94; C $^{\delta}$ H $_3$ 0.85
P60		4.38	2.30, 1.89	C $^{\gamma}$ H 2.05, 1.98; C $^{\delta}$ H 3.88, 3.68
E61	8.29	4.23	2.00, 1.96	C $^{\gamma}$ H 2.47, 2.47
E62	8.25	4.26	1.94	C $^{\gamma}$ H 2.31, 2.26
Y63 c	8.06	4.61	3.09, 2.93	C $^{\delta}$ H 7.11; C $^{\epsilon}$ H 6.79
L64	7.98	4.34	1.59, 1.59	C $^{\gamma}$ H 1.52; C $^{\delta}$ H 0.90, 0.85
Q65	8.13	4.33	2.19, 1.98	C $^{\gamma}$ H 2.35, 2.35
(B) Lys-47 \rightarrow Glu Mutant Hirudin d				
Y3	8.32	4.85	2.81,* 2.63	C $^{\delta}$ H 7.03; C $^{\epsilon}$ H 6.65
T4	8.83	4.66	4.41	C $^{\gamma}$ H $_3$ 1.19
D5	8.92	4.98	2.91,* 2.77	
C6	8.83	4.53	3.10,* 2.63	
E8	7.54	4.67	2.07, 1.79	C $^{\gamma}$ H 2.45, 2.45
S9	8.98	4.85	4.02,* 3.94	
Q11	7.45	4.95	2.31, 2.14	C $^{\gamma}$ H 2.77, 2.61; NH $_2$ 7.69, 6.99

Table I (Continued)

residue	chemical shift (ppm)			
	NH	C α H	C β H ^a	others ^b
N12	8.02	4.58	3.02, 2.88	NH ₂ 7.33, 6.19
L13	9.11	3.34	2.12, 2.12	C γ H 1.63; C δ H ₃ 0.99, 0.90
C14	7.25	5.02	3.27,* 3.16	
C16	7.51	4.72	3.79, 2.83	
C22	8.40	5.14	2.94, 3.14	
N26	7.95	5.48	2.76,* 2.66	NH ₂ 6.75, 6.11
K27	9.19	4.43	1.30, 1.25	C γ H 1.55, 1.03; C δ H 1.46, 1.39; C ϵ H 2.82, 2.72; N δ H 7.58
C28	8.99	5.38	2.96,* 2.82	
L30	8.35	4.17	1.57, 1.57	C γ H 1.43; C δ H ₃ 0.61, 0.61
C39	8.93	5.46	3.12, 2.78*	
T41	8.27	4.45	4.05	C γ H ₃ 1.29
G42	8.26	4.08, 3.72		
E43	7.89	4.26	1.97, 1.97	C γ H 2.58, 2.50
G44	7.89	4.40, 3.63		
T45	8.06	4.80	4.03	C γ H ₃ 1.21
P46		4.66	2.27, 1.94	C γ H 2.06; C δ H 3.92, 3.77
E47	8.43	4.57	2.08, 1.91	C γ H 2.50, 2.50
P48		4.42	2.30, 1.91	C γ H 2.00, 1.96; C δ H 3.88, 3.66
Q49	8.43	4.35	2.10, 1.97	C γ H 2.42, 2.42; NH ₂ 7.62, 6.86
S50	8.26	4.40	3.86, 3.82	
H51	8.54	4.72	3.29, 3.16	C δ 2H 7.29; C ϵ 1H 8.61
N52	8.44	4.71	2.84, 2.75	

^aAn asterisk indicates that the chemical shift corresponds to the C β 3H and the other value to the C β 2H proton (IUPAC notation). ^bA plus indicates that the chemical shift belongs to the C γ 1H proton and the other value to the C γ 2H proton (IUPAC notation). ^cThe chemical shifts of the C β H and C ϵ H protons of Tyr-63 are different from those in natural hirudin purified from the leech (Sukumaran et al., 1987). This is due to the fact that Tyr-63 is sulfated in natural hirudin and unsulfated in recombinant hirudin. ^dOnly those residues for which the chemical shift difference between the wild-type and mutant hirudins for one or more protons is greater or equal to 0.03 ppm are listed.

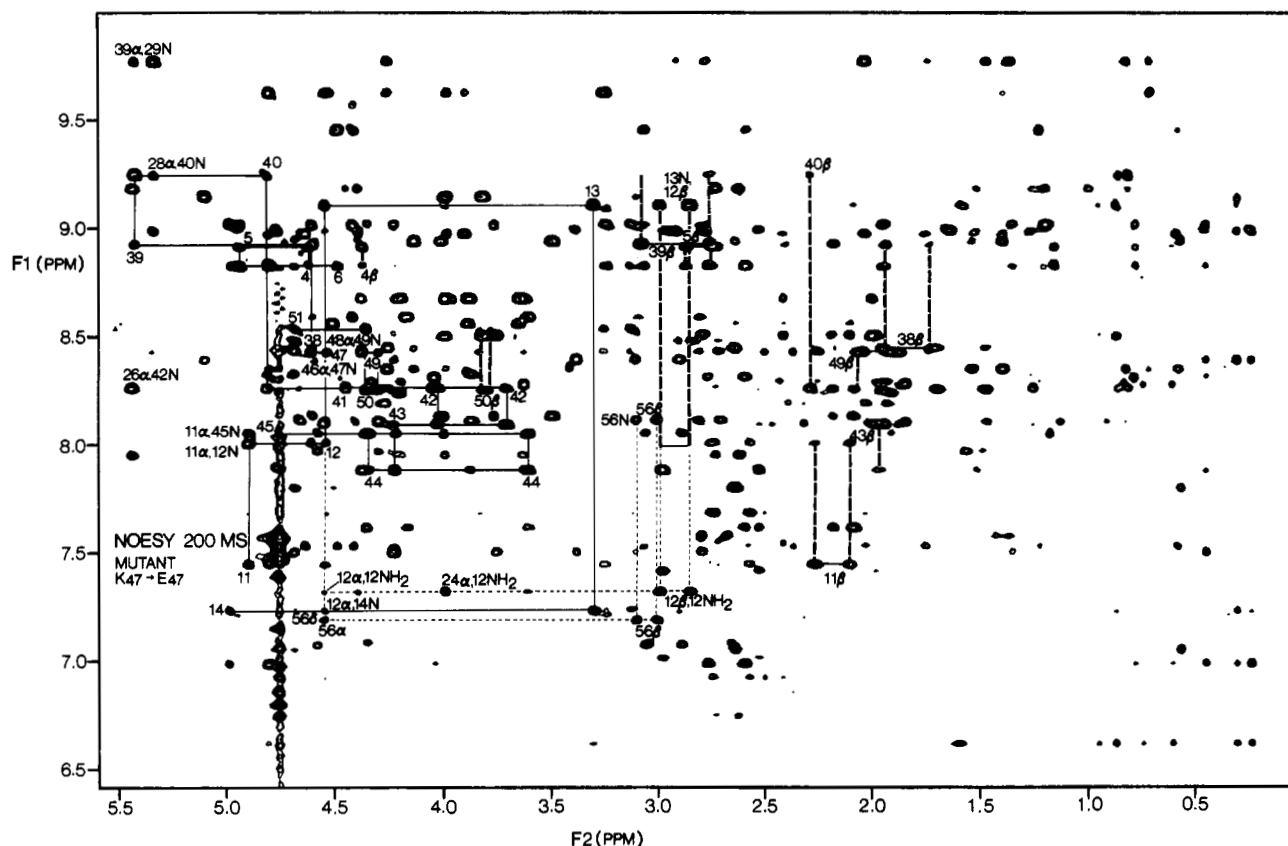


FIGURE 2: NH/aromatic (F1 axis)–aliphatic (F2 axis) region of the 200-ms NOESY spectrum of recombinant mutant hirudin in H₂O at 27 °C. The sequences of $d_{\alpha N}(i,i+1)$ connectivities extending from residues 4–6, 11–13, and 39–51 are indicated by continuous lines, and the peaks are labeled at the positions of the intrareidue NH(i)–C α H(i) cross-peaks. Some $d_{\beta N}(i,i+1)$ connectivities are indicated by dashed lines. Connectivities involving Asn-12 NH₂ and Phe-56 C δ H are shown as dotted lines. Also labeled are a few long-range NH–C α H connectivities.

Stereospecific assignments were made for β -methylene protons as well as for the γ -methyl groups of valines. This involved evaluation of $^3J_{\alpha\beta}$ coupling constants obtained from an E-COSY spectrum and of the relative intensities in the 50-ms NOESY spectra of intrareidue NOEs from the NH

and C α H protons on the one hand to the two C β H protons on the other, and in the case of valine residues to the two C γ H₃ protons (Hyberts et al., 1987; Wagner et al., 1987; Zuiderweg et al., 1985). All stereospecific assignments are included in Table I.

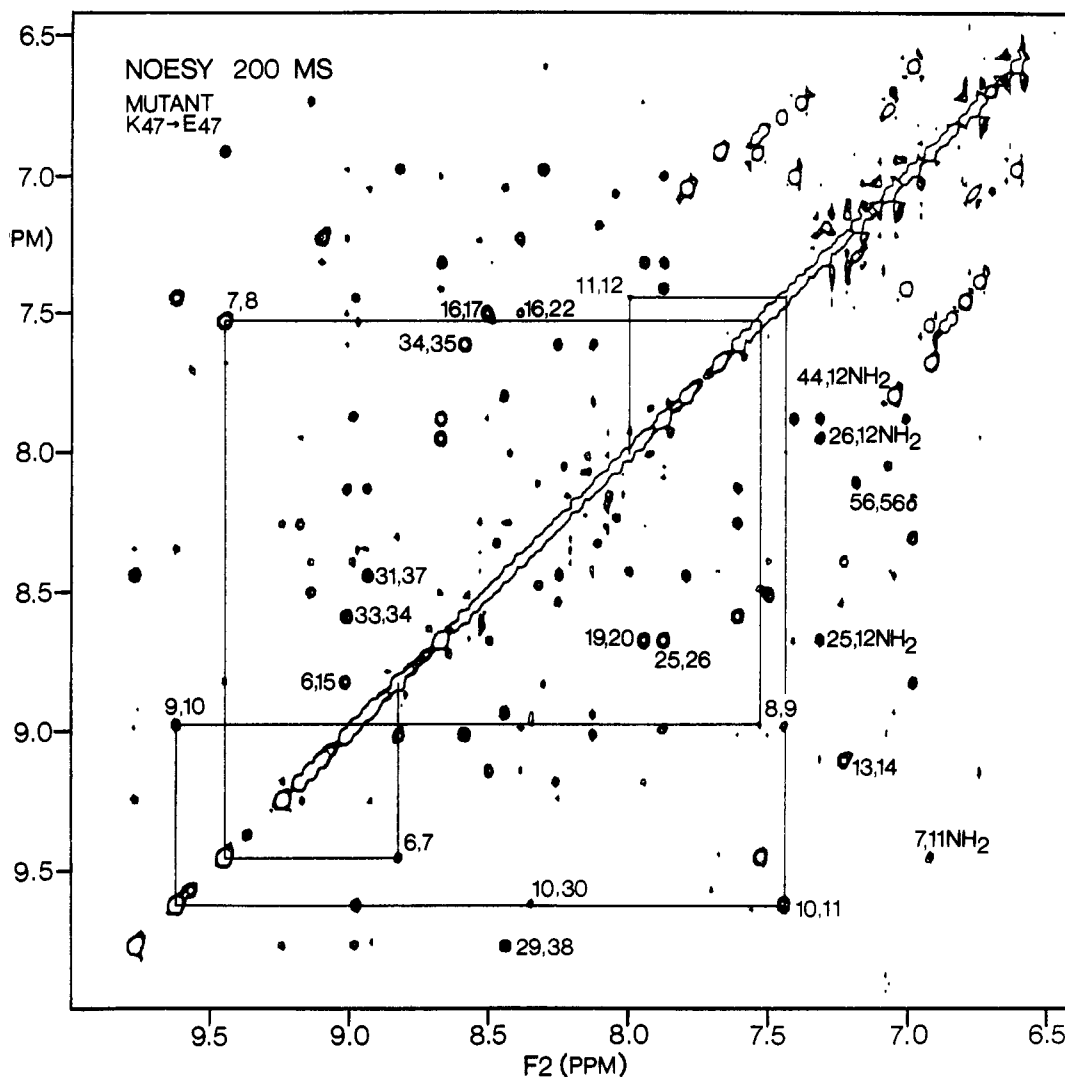


FIGURE 3: NH (F1 axis)–NH (F2 axis) region of the 200-ms NOESY spectrum of recombinant mutant hirudin in H₂O at 27 °C. The sequence of $d_{NN}(i,i+1)$ connectivities extending from residue 7 to residue 12 as well as some long-range connectivities are indicated.

There are a large number of long-range ($|i - j| > 5$) interresidue NOEs involving residues between positions 3 and 48. In contrast, only intraresidue and sequential ($i,i+1$) NOEs were observed for the polypeptide chain extending from residue 49 to residue 65. We therefore conclude that there is no evidence that the C-terminus (residues 50–65) has an ordered structure or folds back onto the rest of the protein. The high degree of NH chemical shift degeneracy over a range of temperature and the absence of slowly exchanging amide protons are consistent with a “random-coil” structure for this portion of the molecule. Consequently, the structure calculations presented in the following sections were restricted to the N-terminal 49 residues.

The conclusion concerning the C-terminus is in disagreement with that of our previous paper (Sukumaran et al., 1987; Clore et al., 1987a) where five NOEs between Ser-9 and Gln-57, Thr-7 and Phe-56, Asn-12 and Phe-56, and Cys-28 and Phe-56 suggested folding back to the C-terminus. In light of the reassignments pointed out above, however, the NOEs previously thought to connect the C^βH protons of Phe-56 and the two C^βH protons of Asn-12 are actually intraresidue C^βH–C^βH connections of Phe-56. The two NOE connections from the NH protons of Thr-7 and Cys-28 to the C^βH protons of Phe-56, on the other hand, were no longer apparent in the spectra of the two recombinant hirudins. To exclude the possibility that there is a difference between natural (sulfated

Tyr-63) and wild-type recombinant (unsulfated Tyr-63) hirudin in this respect, we recorded both HOHAHA and NOESY spectra at 600 MHz in H₂O on a sample of natural hirudin. No connection between Thr-7 or Cys-28 and Phe-56 could be detected in the 600-MHz spectra of natural hirudin. Reexamination of the 500-MHz natural hirudin data indicated that these “NOEs” arose from artifact ridges in the spectrum that could be suppressed with the processing protocol described under Experimental Procedures. Finally, the previously reported NOEs between the C^αH proton of Glu-57 and the C^αH and C^βH protons of Ser-9 have been reassigned to NOEs between Ser-9 and Ile-29. In this respect, we note that the C^αH protons of Ile-29 and Glu-57 are degenerate in both the wild-type and mutant hirudin. The observation, however, of NOEs between the C^βH protons of Ser-9 and the C^γH₃ and C^δH₃ protons of Ile-29, together with the presence of a number of NOEs between Glu-8, Ser-9, and Gly-10 on the one hand and Leu-30 on the other, as well as the absence of any other potential long-range NOEs involving Glu-57, makes the previous assignment highly improbable. This was confirmed by the structure calculations which indicated that the new assignment was completely consistent with all the other NOEs.

Our observation regarding the C-terminus of hirudin is supported by biochemical studies which showed that the C-terminal 22 residues of hirudin are freely accessible to enzyme digestion, while the N-terminal part of hirudin containing the

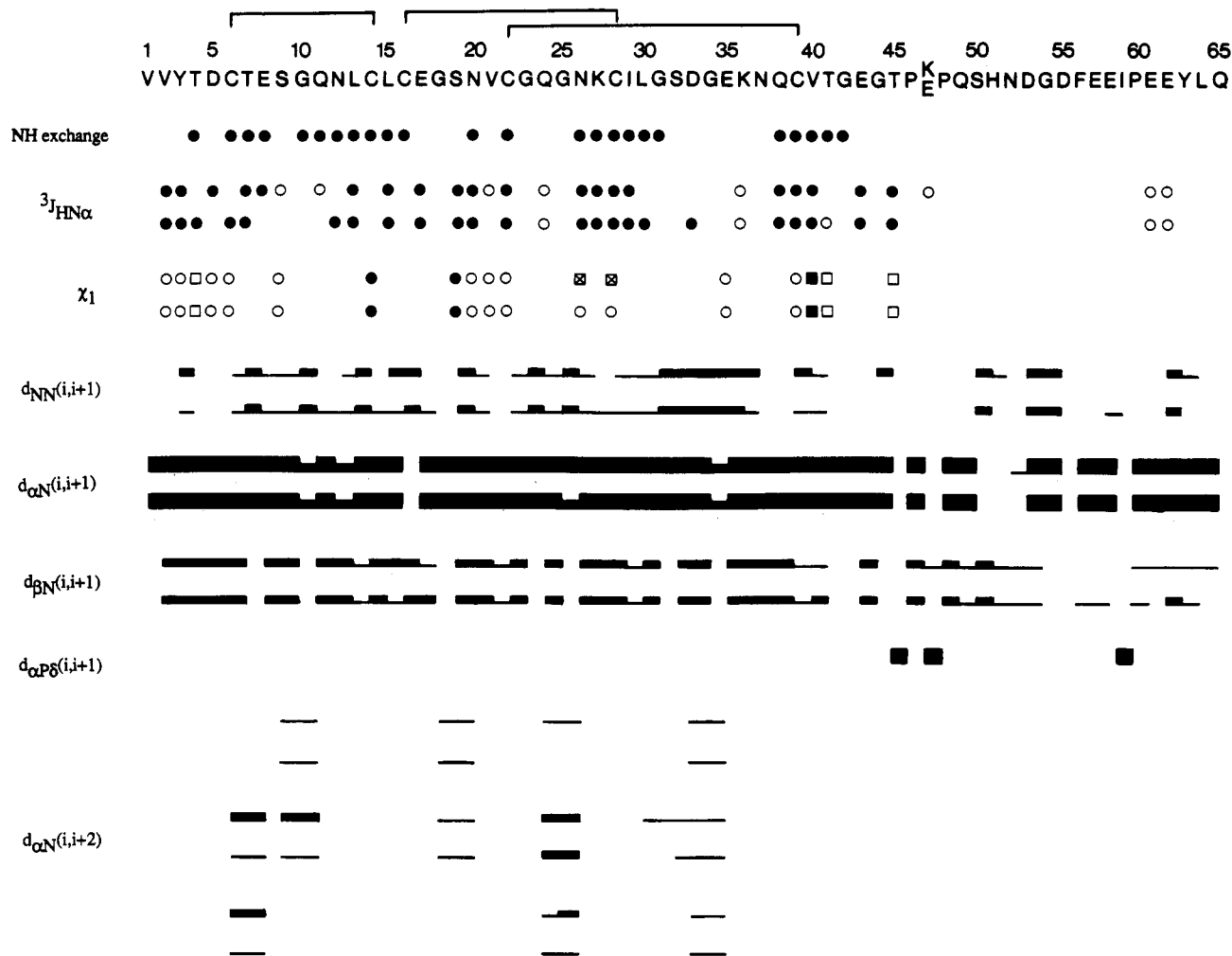


FIGURE 4: Sequence of both wild-type and mutant hirudins with a summary of all the short-range NOEs involving the NH, C^αH, and C^βH protons, as well as the C^βH protons of proline residues, the slowly exchanging NH protons, the ³J_{HN α} coupling constants, and the χ_1 side-chain torsion angles. In the case of differences between the two hirudins, the data for the wild-type appear above those for the mutant. The NOEs are classified as strong, medium, and weak by the thickness of the line. NH protons that are still present after 12 h of the protein being dissolved in D₂O are indicated by closed circles. ³J_{HN α} coupling constants >8 Hz are indicated by closed circles (●) and those <7 Hz by open circles (○). The ranges for the χ_1 side-chain torsion angles, derived from the ³J _{$\alpha\beta$} coupling constants and the pattern of intraresidue NH–C^αH and NH–C^βH NOEs, are as follows: (●) 0° < χ_1 < 120°; (■) 120° < χ_1 < 240°; (○) –120° < χ_1 < 0°; (□) 0° < χ_1 < 240°; (crossed box) –240° < χ_1 < 0°. The location of the disulfide bridges is indicated above the sequence.

disulfide bridges is not (Chang, 1983; Dodt et al., 1987). Other experiments with synthetic peptides have shown that unsulfated N^α-acetylhirudin_{45–65} binds to α -thrombin with an association constant of $\sim 10^5$ M⁻¹ at a site distinct from the catalytic site and that this interaction principally involves residues 54–65 (Krstenansky & Mao, 1987; Owen et al., 1988). This suggests that the interaction of the C-terminus with the core of hirudin is not necessary for binding. The mode of interaction of the N-terminal part of hirudin with thrombin is unknown, although it must clearly contribute significantly to the binding energy, as wild-type hirudin binds to thrombin with an association constant 5–6 orders of magnitude larger than that of the C-terminal synthetic peptides.

A number of other long-range NOEs have also been reassigned on the basis of the study of the two recombinant proteins. The NOEs connecting the amide NH protons of residues 25, 26, 28, and 44 with the amide NH of Glu-8 (Sukumaran et al., 1987) are shown instead to be connected to an NH₂ side-chain amide proton of Asn-12 (Figure 3). The incorrect assignment was made before, partly because of the incorrect assignments involving Asn-12 and Phe-56 (see above), and the error was compounded by the degeneracy of the Glu-NH and Asn-12 side-chain NH₂ resonances in the spectrum of natural

hirudin [see Figure 3 of Sukumaran et al. (1987)]. This degeneracy is alleviated in the spectrum of the mutant hirudin where the chemical shifts of the Glu-8 NH and Asn-12 NH₂ resonances differ by 0.21 ppm (see Figure 3). Additionally, the NH–NH NOE previously assigned to a long-range connection between residues 10 and 28 is now known to represent a sequential $d_{\text{NN}}(i,i+1)$ NOE between residues 9 and 10. In Figure 3 a number of long-range NH–NH NOEs are indicated.

Structure Determination. As no long-range NOEs were observed for the C-terminal residues, structures were computed for the N-terminal part of both hirudins up to residue 49. The calculations were carried out with a set of 685 and 661 structurally useful NOEs for the wild-type and mutant hirudin, respectively. For the wild-type hirudin these consisted of 242 short-range ($|i - j| \leq 5$, where i and j are residue numbers) and 208 long-range ($|i - j| > 5$) interresidue NOEs and 235 intraresidue NOEs; for the mutant hirudin they comprised 234 short-range ($|i - j| \leq 5$) and 199 long-range ($|i - j| > 5$) interresidue NOEs and 228 intraresidue NOEs. These NOEs were first identified in 200-ms NOESY spectra and then classified into three distance ranges, 1.8–2.7, 1.8–3.3, and 1.8–5.0 Å, corresponding to strong, medium, and weak NOEs

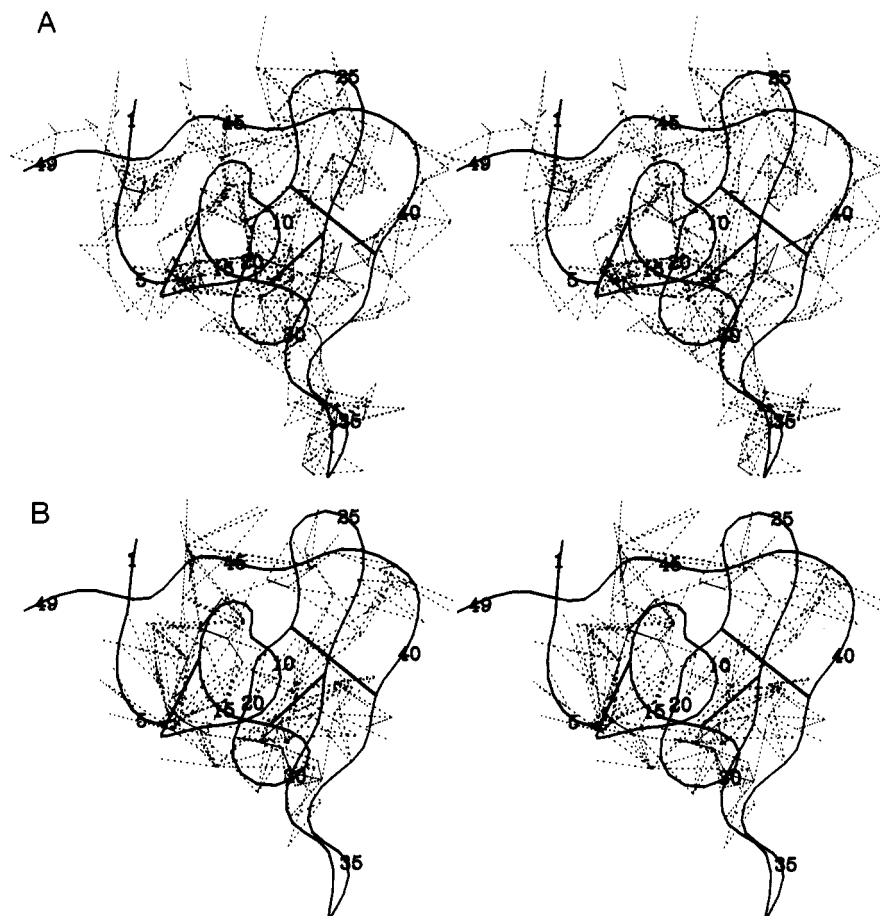


FIGURE 5: (A) Intrasidue and short-range interresidue ($|i - j| \leq 5$) and (B) long-range interresidue ($|i - j| > 5$) interproton distance restraints shown as dashed lines superimposed on a framework comprising a smoothed backbone (N, C $^{\alpha}$, C) atom representation of the restrained minimized average structure ($\overline{SA_{w,r}}$). The three disulfide bridges between residues 6 and 14, 16 and 28, and 22 and 39 are shown as straight lines connecting the corresponding C $^{\alpha}$ atoms.

in the shorter mixing time NOESY data (Williamson et al., 1985; Clore et al., 1986b). The upper limits of distances involving methylene protons which were not stereospecifically assigned, methyl protons, and the C $^{\beta}$ H and C $^{\gamma}$ H protons of Tyr and Phe were corrected for centre (r_c) averaging (which is equivalent to the use of pseudoatoms) as described by Wüthrich et al. (1983). In the case of NOEs involving methyl groups, an additional 0.5 Å per methyl group was also added to the upper distance limit to account for the higher apparent intensity of the methyl resonance (Wagner et al., 1987; Clore et al., 1987b).

A superposition of the interproton distance restraints on a smooth backbone atom representation of one of the calculated structures is shown in Figure 5. The number of NOE restraints used in the present calculations represents a significant increase over the number used in the previous study, namely, a total of 329 restraints for residues 1–49, comprising 126 short- and 60 long-range interresidue distances and 141 intrasidue distances (Clore et al., 1987a). Thus, the number of long-range interresidue restraints has more than tripled while the number of short-range interresidue restraints and intrasidue restraints has approximately doubled. In this respect, the improved quality of the 600-MHz spectra in terms of increased sensitivity, line shape and stability, coupled with a concomitant reduction in instrumental artifacts (e.g., t_1 noise), played a major role. This is easily appreciated by comparing the 600-MHz NOESY spectra in Figures 2 and 3 of the present paper with the 500-MHz NOESY spectra in Figures 3 and 4 of the previous paper (Sukumaran et al.,

1987). The NH–NH region illustrates this in a particularly obvious way, where simple visual inspection reveals that there are about twice as many NOE cross-peaks in the 600-MHz spectrum (Figure 3) compared to the 500-MHz spectrum [Figure 3 of Sukumaran et al. (1987)].

In addition to the NOE distance restraints, 16 distance restraints for 8 backbone NH–CO hydrogen bonds were included in the input distance restraints list [$r_{N(i)-O(j)} \leq 3.3$ Å and $r_{NH(i)-O(j)} \leq 2.3$ Å for each hydrogen bond]. These were identified according to the criteria laid out by Wagner et al. (1987) which consist of the presence of NOEs between residues on opposite strands of an antiparallel β -sheet in conjunction with the existence of a slowly exchanging backbone NH proton. The NH(i)–CO(j) backbone hydrogen bonds identified in this manner were as follows: (i,j) = (27,40), (40,27), (29,38), (38,29), (31,36), (35,32), (20,17), and (16,20), where i and j represent the residue numbers of the two amino acids involved. These hydrogen bonds occur in the two regions (residues 16–22 and 26–42) of regular secondary structure identified previously, each consisting of a two-stranded antiparallel β -sheet connected by a β -turn (Sukumaran et al., 1987).

In the distance geometry phase of the calculations, nine distance restraints were included to define the three disulfide bridges between Cys-6 and Cys-14, Cys-16 and Cys-28, and Cys 22 and Cys 39. For each disulfide bridge these are $r_{S(i)-S(j)} = 2.02 \pm 0.05$ Å, $r_{C\beta(i)-S(j)} = 2.99 \pm 0.05$ Å, and $r_{C\beta(j)-S(i)} = 2.99 \pm 0.05$ Å. In the dynamical simulated annealing stage, restraints for the disulfide bridges were explicitly included in

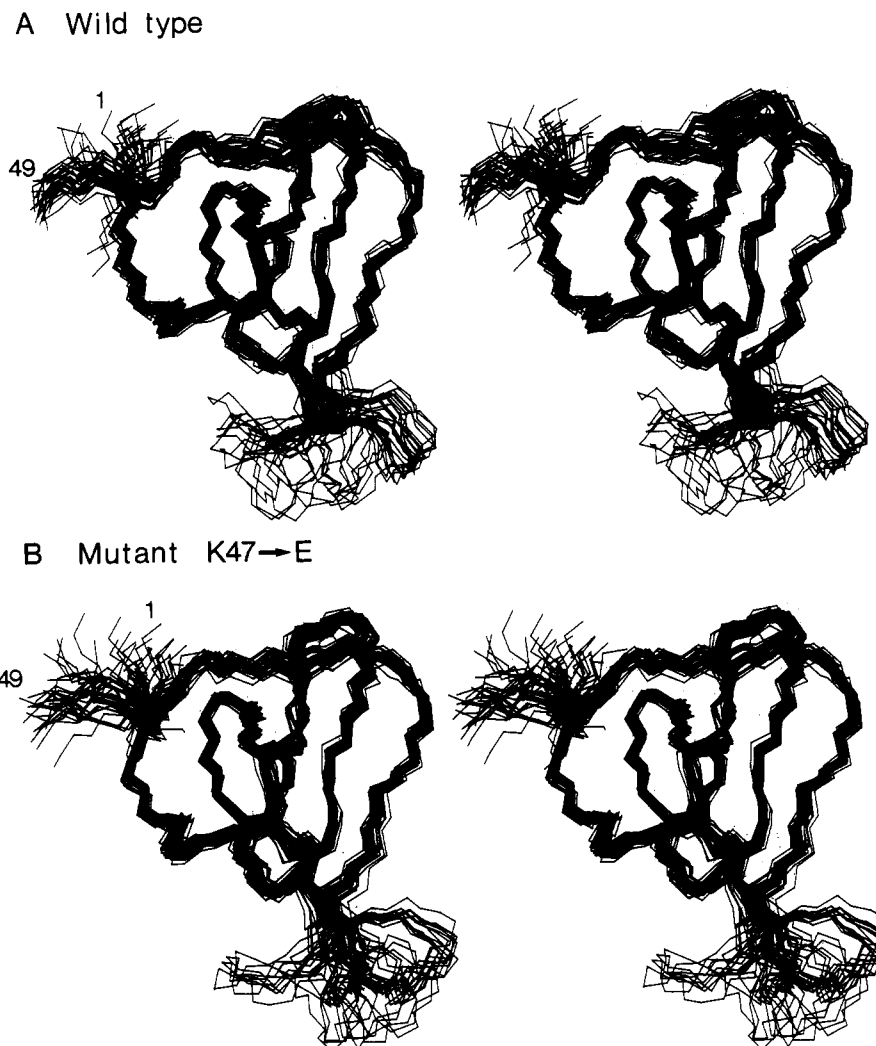


FIGURE 6: Stereoviews showing best-fit superpositions of the backbone (N, C $^{\alpha}$, C) atoms of the 32 (SA $_{wt}$) (A) and 32 (SA $_{mut}$) (B) structures. The structures are best fitted to residues 2–30 and 38–48.

bond and angle terms describing the covalent geometry.

A total of 26 ϕ backbone torsion angle restraints were derived from $^3J_{HN\alpha}$ coupling constants measured from the COSY spectra in H $_2$ O. ϕ angles were restrained to ranges of $-160^\circ < \phi < -80^\circ$ and $-90^\circ < \phi < -40^\circ$ on the basis of $^3J_{HN\alpha}$ coupling constant values of >8.0 Hz and <7.0 Hz, respectively (Pardi et al., 1984). A total of 18 χ_1 side-chain torsion angle restraints were derived on the basis of $^3J_{\alpha\beta}$ coupling constants and the relative intensities of the two NH–C $^{\beta}$ H NOEs and of the two C $^{\alpha}$ H–C $^{\beta}$ H NOEs in the 50-ms NOESY spectra (Wagner et al., 1987). A summary of the ϕ and χ_1 torsion angle restraints is given in Figure 4.

A total of 32 structures were computed for both the wild-type and mutant hirudin and are referred to as (SA $_{wt}$) and (SA $_{mut}$), respectively. The structural statistics for these structures, as well as for the mean and restrained minimized mean structures, are given in Table II, and various atomic rms differences are given in Table III. Best-fit superpositions of the backbone atoms of the 32 wild-type and 32 mutant structures are shown in Figure 6 and plots of atomic rms distribution as a function of residue number in Figure 7. The final dynamical simulated annealing structures and the restrained minimized mean structures, (SA $_{wt}$) $_r$ and (SA $_{mut}$) $_r$, satisfy the experimental restraints, display very small deviations from idealized covalent geometry, and possess good nonbonded contacts as evidenced by small values for the van der Waals repulsion term F_{repel} and negative values of the Lennard–Jones

van der Waals energy (Table II).

It is clear from Figures 6 and 7 that the backbone conformation of the N-terminal core formed by residues 2–30 and 37–48 is very well determined with a backbone atomic rms difference between the individual structures and the mean structure obtained by averaging their coordinates, best fitted to residues 2–30 and 37–48, of only 0.67 ± 0.10 and 0.64 ± 0.09 Å for the wild-type and mutant hirudin, respectively (Table III).

The core is principally stabilized by the three disulfide bridges between Cys-6 and Cys-14, Cys-16 and Cys-28, and Cys-22 and Cys-39. The first five residues form an irregular strand which leads into a loop closed off at its base by the disulfide bridge between Cys-6 and Cys-14. This is followed by a miniantiparallel β -sheet formed by residues 14–16 (strand I) and 21–22 (strand I') connected by a type II turn (residues 17–20). This β -sheet is distorted by a β -bulge (Richardson, 1981) at Cys 16, which was correctly predicted previously on the basis of a qualitative interpretation of the NOE data (Sukumaran et al., 1987). Strand I' leads into the second antiparallel β -sheet formed by residues 27–31 (strand II) and 36–40 (strand II') connected by a β -turn (residues 32–35). Additionally, residues 10–11 exhibit features of a β -bulge with the amide of Gly-10 and the carbonyl oxygen atom of Glu-11 hydrogen bonded to the carbonyl and amide groups, respectively, of Cys 28. A more detailed view of the two regular secondary structure elements within the core showing best-fit

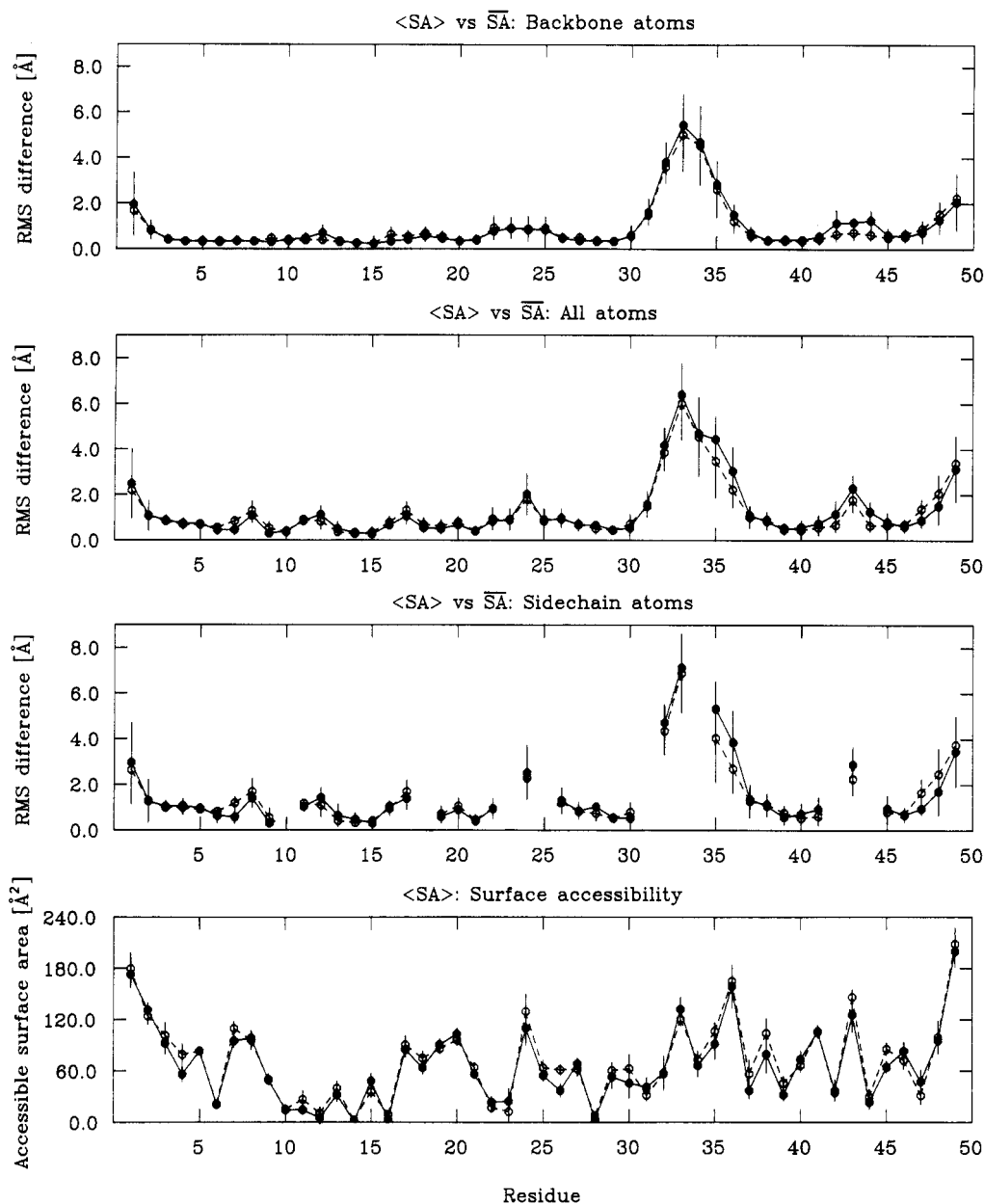


FIGURE 7: Atomic rms distribution of the 32 individual ($\langle SA_{wt} \rangle$) and 32 individual ($\langle SA_{mut} \rangle$) structures about the mean structures \overline{SA}_{wt} and \overline{SA}_{mut} , respectively, best fitted to residues 2–30 and 38–48, and surface accessibility. The average rms difference at each residue between the individual ($\langle SA_{wt} \rangle$) and ($\langle SA_{mut} \rangle$) structures and their respective mean structures are represented by filled (●) and open (○) circles, respectively; the bars represent the standard deviations in these values and similarly for the surface accessibility.

superpositions of the backbone (N, C $^{\alpha}$, C, O) atoms of the 32 wild-type structures is shown in Figure 9. All the backbone hydrogen bonds depicted in Figure 8 are associated with slowly exchanging backbone amide protons (Figure 4). As described previously (Clare et al., 1987a) residues 31–36 form an exposed finger of antiparallel β -sheet, whose orientation with respect to the core cannot be determined on the basis of the present data (Figure 6). This is due to the fact that no long-range NOEs from residues 31–36 to the core could be detected (cf. Figure 5B). Nevertheless, a best-fit superposition of residues 31–36 of the 32 wild-type structures shows that locally, at least, the approximate polypeptide fold in this region is reasonably well defined, despite the obvious existence of local mirror images (see supplementary material). The exposed nature of residues 31–36 is further supported by the absence, with the exception of Gly-31, of any slowly exchanging backbone amide protons within this region, despite the fact that the NOE data are clearly indicative of a β -sheet and turn. Finally, strand

II' leads into an irregular strand which folds back onto the protein such that residue 47 (Lys in the wild type and Glu in the mutant) is in close proximity to residues in the loop closed off by the disulfide bridge between Cys-6 and Cys-14. Thus, in both wild-type and mutant hirudin long-range NOEs were found from Thr-7, Gln-11, and Cys-14 to Lys-47/Glu-47, from Gln-11 to Thr-45 and Pro-48, from Asn-12 to Gly-44, and from Leu-13 to Pro-46.

It is informative, in the light of the reassignments presented above, to compare the structure of the protein core determined in this study with that determined previously (Sukumaran et al., 1987; Clare et al., 1987a). Residues 56 and 57 which were thought to form part of the core previously are now part of an apparently disordered C-terminal tail. From a qualitative viewpoint the two elements of regular secondary structure are unchanged. The orientation and twist of residues 18–25 (i.e., the turn following strand I, strand I', and the segment connecting strand I' and strand II) are altered. In particular, the

Table II: Structural Statistics^a

	wild-type hirudin ₁₋₄₉			Lys47 → Glu mutant (1-49)		
	$\langle SA_{wt} \rangle$	\overline{SA}_{wt}	$(\overline{SA}_{wt})_r$	$\langle SA_{mut} \rangle$	\overline{SA}_{mut}	$(\overline{SA}_{mut})_r$
rms deviations from experimental restraints (Å) ^b						
all (701/677)	0.088 ± 0.004	0.092	0.075	0.077 ± 0.003	0.078	0.071
interresidue						
short range ($ i - j \leq 5$) (242/234)	0.109 ± 0.009	0.102	0.094	0.092 ± 0.006	0.099	0.083
long range ($ i - j > 5$) (208/199)	0.077 ± 0.005	0.053	0.057	0.066 ± 0.004	0.048	0.068
intraresidue (235/228)	0.068 ± 0.006	0.100	0.067	0.067 ± 0.006	0.079	0.062
H bond (16/16) ^c	0.102 ± 0.020	0.083	0.052	0.083 ± 0.019	0.037	0.039
F_{NOE} (kcal·mol ⁻¹) ^d	262 ± 51	293	196	201 ± 13	208	170
F_{tor} (kcal·mol ⁻¹) ^e	22 ± 15	74	14	12 ± 6	346	16
F_{repel} (kcal·mol ⁻¹) ^f	66 ± 10	14061	45	42 ± 5	8839	49
F_{L-J} (kcal·mol ⁻¹) ^g	-58 ± 18	>10 ⁶	-73	-66 ± 11	>10 ⁶	-73
deviations from idealized geometry ^h						
bonds (Å) (676/669)	0.014 ± 0.001	0.456	0.012	0.011 ± 0.001	0.448	0.011
angles (deg) (1223/1208)	2.582 ± 0.514	27.874	1.814	2.754 ± 0.760	29.278	3.177
impropers (deg) (131/132)	0.717 ± 0.075	1.829	0.597	0.609 ± 0.054	4.899	0.419

^aThe notation of the structures is as follows: $\langle SA_{wt} \rangle$ are the 32 final dynamical simulated annealing wild-type structures and $\langle SA_{mut} \rangle$ are the 32 final dynamical simulated annealing Lys-47 → Glu mutant hirudin structures; \overline{SA}_{wt} and \overline{SA}_{mut} are the mean structures obtained by averaging the coordinates of the respectively individual SA structures best fitted to residues 2-30 and 37-48; $(\overline{SA}_{wt})_r$ and $(\overline{SA}_{mut})_r$ are the structures obtained by restrained minimization of \overline{SA}_{wt} and \overline{SA}_{mut} , respectively. ^bThe rms deviations from the experimental restraints are calculated with respect to the upper and lower limits of the distance restraints (Clore et al., 1986b). None of the structures exhibited violations greater than 0.5 Å. The number of distances in each category is given in parentheses next to the category name, the first number referring to the wild-type hirudin and the second to the mutant. ^cFor each backbone hydrogen bond there are two restraints: $r_{NH-O} < 2.3$ Å and $r_{N-O} < 3.3$ Å. The lower limits are given by the sum of the van der Waals radii of the relevant atoms. Eight backbone hydrogen bonds within regular elements of secondary structure were identified on the basis of the NOE and NH exchange data [see text and Sukumaran et al. (1987)]. ^dThe values of the square-well NOE potential F_{NOE} (eq 4) are calculated with a force constant of 50 kcal·mol⁻¹·Å⁻⁴. ^eThe values of F_{ϕ} are calculated with a force constant of 200 kcal·mol⁻¹·rad⁻². F_{ϕ} is a square-well dihedral potential (eq 5) which is used to restrict the ranges of ϕ and χ_1 torsion angles as indicated in Figure 5. There are 26 ϕ backbone and 18 χ_1 side-chain torsion angle restraints for both the wild-type and mutant hirudins. ^fThe values of the van der Waals repulsion term F_{repel} (cf. eq 3) are calculated with a force constant of 4 kcal·mol⁻¹·Å⁻⁴ with the hard-sphere van der Waals radii set to 0.8 times the standard values used in the CHARMM empirical energy function (Brooks et al., 1983). ^g F_{L-J} is the Lennard-Jones van der Waals energy calculated with the CHARMM empirical energy function (Brooks et al., 1983). ^hThe number of bond, angle, and improper terms is given in parentheses, the first number referring to the wild-type hirudin and the second to the mutant. The improper terms serve to maintain planarity and appropriate chirality; they also maintain the peptide bond of all residues in the trans conformation. In the dynamical simulated annealing calculations, the restraints for the disulfide bridges are included in the bond and angle terms.

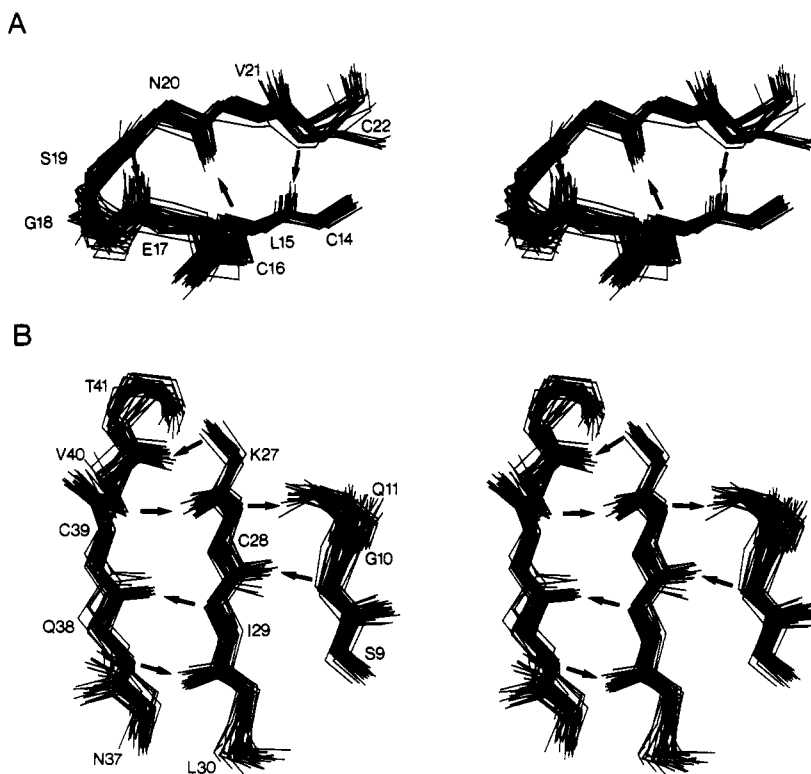


FIGURE 8: Stereoviews showing best-fit superpositions of the backbone (N, C α , C, O) atoms of the 32 (SA_{wt}) structures for the two regions of regular secondary structure. Backbone hydrogen bonds are shown as arrows with the direction of the arrow from the N to the O atom. (A) Residues 14-22; (B) residues 9-11, 27-30, and 37-41.

left-handed twist of this segment in the previous structure is converted to a right-handed twist, characteristic of a β -sheet

(Richardson, 1981), in the present structure, and its orientation relative to the rest of the core is altered by $\sim 90^\circ$. This change

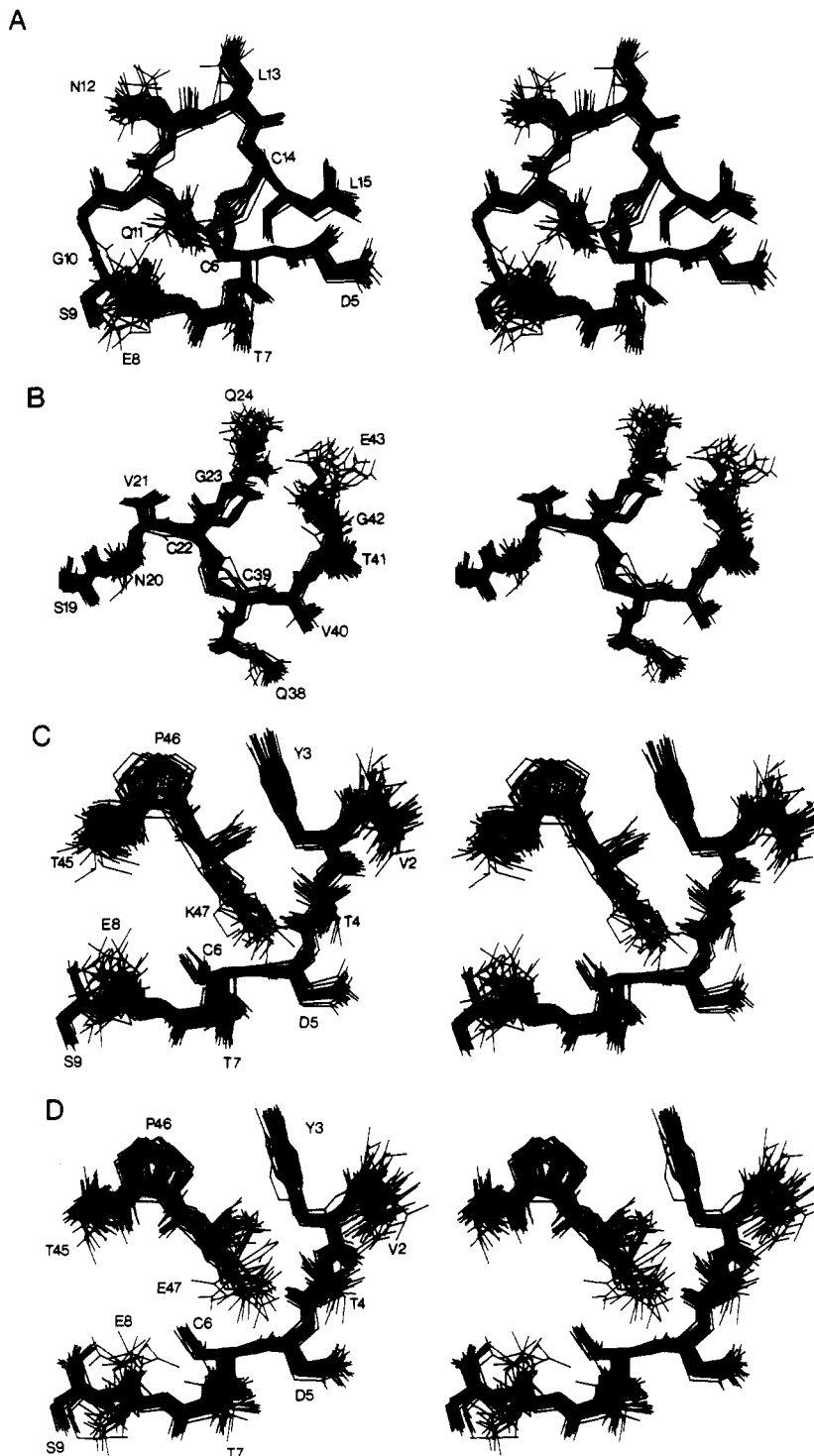


FIGURE 9: Stereoviews showing best-fit superposition of all atoms (excluding protons) of the 32 (SA_{wt}) structures for three selected segments of the protein. (A) Residues 5-15; (B) residues 19-24 and 38-43; (C) residues 2-9 and 45-47; (D) as in (C) but for the 32 (SA_{mut}) structures.

is driven in part by the reassignment of the long-range NOEs described above, particularly those between the Asn-12 NH_2 and the NH s of residues 25, 26, 28, and 44, as well as by new additional NOEs. Excluding this segment, the best-fit atomic rms difference between the old and new average restrained minimized structures for the core residues (i.e., residues 3-17, 26-30, and 37-46) is $\sim 3.4 \text{ \AA}$, which is approximately the same value as that of the average pairwise atomic rms differences between the old individual restrained dynamics structures.

The conformations of many side chains within the core are also reasonably well determined with an average all atom rms

difference of $\sim 1 \text{ \AA}$ between the individual structures and the mean structure for both the wild-type and mutant hirudin. This is evident not only from the atomic rms distribution plots (Figure 7) but also from the superpositions of all atoms (excluding protons) of the 32 wild-type structures for selected regions shown in Figure 9. This is noteworthy as the majority of residues have high surface accessibilities with only the six cysteine residues and 14 others having surface accessibilities less than 50 \AA^2 . Some degree of correlation between side-chain definition and surface accessibility is apparent (Figure 7) and simply reflects the reduced density of short ($< 5 \text{ \AA}$) interproton distances.

Table III: Atomic rms Differences^a

structures	atomic rms differences (Å)			
	residues 1-49		residues 2-30 and 37-48	
	backbone atoms	all atoms	backbone atoms	all atoms
wild-type hirudin				
$\langle \overline{SA}_{wt} \rangle$ vs \overline{SA}_{wt} ^b	1.37 ± 0.21	1.81 ± 0.21	0.67 ± 0.10	0.98 ± 0.12
$\langle \overline{SA}_{wt} \rangle$ vs $\langle \overline{SA}_{wt} \rangle$ ^{b,c}			0.96 ± 0.15	1.42 ± 0.20
$\langle \overline{SA}_{wt} \rangle$ vs $\langle \overline{SA}_{wt} \rangle$ r	1.53 ± 0.29	2.00 ± 0.33	0.80 ± 0.10	1.14 ± 0.16
$\langle \overline{SA}_{wt} \rangle$ r vs \overline{SA}_{wt}	0.71	0.96	0.45	0.59
mutant hirudin				
$\langle \overline{SA}_{mut} \rangle$ vs \overline{SA}_{mut} ^b	1.27 ± 0.26	1.68 ± 0.27	0.64 ± 0.09	0.98 ± 0.10
$\langle \overline{SA}_{mut} \rangle$ vs $\langle \overline{SA}_{mut} \rangle$ ^{b,c}			0.92 ± 0.17	1.41 ± 0.18
$\langle \overline{SA}_{mut} \rangle$ vs $\langle \overline{SA}_{mut} \rangle$ r	1.40 ± 0.31	1.87 ± 0.35	0.72 ± 0.09	1.11 ± 0.11
$\langle \overline{SA}_{mut} \rangle$ r vs \overline{SA}_{mut}	0.66	0.88	0.33	0.53
wild-type versus mutant				
$\langle \overline{SA}_{wt} \rangle$ vs $\langle \overline{SA}_{mut} \rangle$ ^d			1.13 ± 0.20	1.62 ± 0.20
\overline{SA}_{wt} vs \overline{SA}_{mut}			0.70	0.87
$\langle \overline{SA}_{wt} \rangle$ r vs $\langle \overline{SA}_{mut} \rangle$ r			0.84	1.18

^aThe notation of the structures is the same as that in Table II. ^bNote that by use of standard statistical theory it is easily shown that the average rms difference between all pairs of SA structures is related to the average rms difference between the individual SA structures and the mean SA structure by a factor of $\sim [2n/(n-1)]^{1/2}$, which in this case is equal to 1.437. ^cThe values given are the averages for 528 pairwise comparisons. ^dThe values given are the averages for 1024 pairwise comparisons.

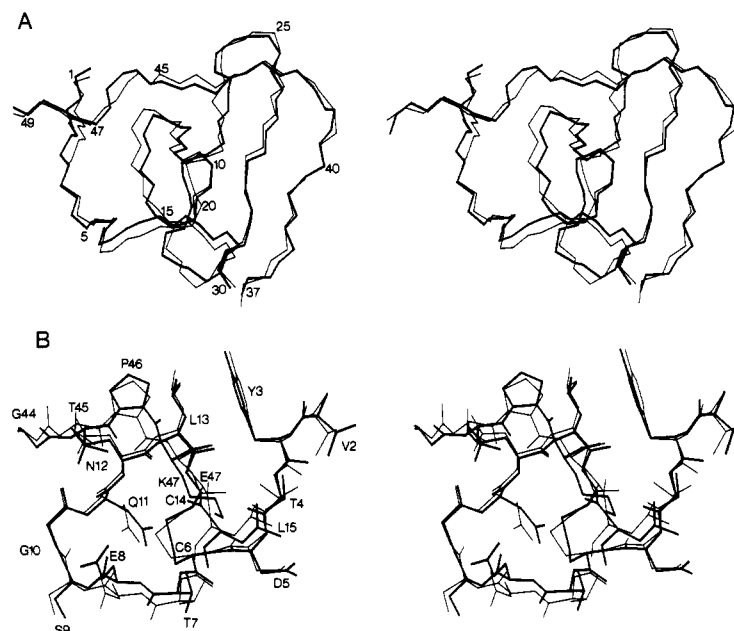


FIGURE 10: Best-fit superpositions of the restrained minimized average structure $\langle \overline{SA}_{wt} \rangle$ r and $\langle \overline{SA}_{mut} \rangle$ r shown as thick and thin lines, respectively. (A) View of the backbone (N, C α , C) atoms of residues 1-30 and 37-49; (B) view of all atoms (excluding protons) of residues 2-15 and 44-47.

Comparison of the Wild-Type and Mutant Structures. Comparison of the stereoviews in Figure 6 indicates that the structures of the wild-type and mutant hirudin are indeed very similar. This is confirmed by the superposition of the core (residues 1-30 and 37-49) of the two restrained minimized mean structures, $\langle \overline{SA}_{wt} \rangle$ r and $\langle \overline{SA}_{mut} \rangle$ r, shown in Figure 10 which provides a good representation of the differences between the two structures. In this respect we note that, of the 1024 pairwise comparisons between the individual $\langle \overline{SA}_{wt} \rangle$ and $\langle \overline{SA}_{mut} \rangle$ structures, there are no pairs with either backbone atom or all atom rms differences smaller than that between the two mean structures, \overline{SA}_{wt} and \overline{SA}_{mut} , and only 3 and 21 pairs with all atom and backbone atom rms differences, respectively, smaller than that between the two restrained minimized mean structures (Table III). This qualitative result was already expected given the close similarity of the chemical shifts and the pattern of both short- and long-range interresidue NOEs between the wild-type and mutant hirudin. A more quantitative assessment of regions of significant difference can

be obtained by comparing the atomic rms distributions about the mean for the individual structures (Figure 7) with the atomic rms difference between the two mean structures (supplementary material). A region of distinct difference is indicated in the case where the latter rms difference is larger than the former. This is the case for the backbone atoms of residues 3, 5, 8, 11 to 15, 22, 26, and 27. In the mutant the backbone atoms of residues 3, 5, and 11-15 are slightly closer to those of residues 45-47 than in the wild-type, a change which can be rationalized in terms of the shorter length of the Glu side chain relative to that of Lys. Concomitantly, the backbone of residue 8 appears to be pushed away. Residues 22, 26, and 27 also move in the same direction as residues 11-15. This is secondary to the perturbation of residues 11-15 and can be attributed to the presence of numerous contacts between residues 8-11 and 28-30, including the hydrogen bonds between Cys-28 and Gly-10 and between Cys-28 and Glu-11 (cf. Figure 8). There seem to be no significant differences, however, with respect to the side-chain positions

within the present errors of the coordinates, even within the immediate vicinity of residue 47. This is clearly evident from structures C and D of Figure 9 which show best-fit superpositions of all atoms of the 32 wild-type and mutant structures, respectively, for residues 2–9 and 45–47 and from Figure 10B which shows a superposition of all atoms of the wild-type and mutant restrained minimized mean structures for residues 2–15 and 44–47.

In contrast to the small structural differences between the wild-type and the mutant, there are quite a number of chemical shift differences between the wild-type and the mutant (Table I). The most significant changes are found in two regions comprising residues 3–14 (excluding residues 7 and 10) and 41–52 and the majority affect principally the NH and C α H protons. The chemical shift changes for the former region can clearly be explained in terms of the small shift in their backbone positions, while those for the latter can probably be attributed to their close proximity in the sequence to the mutated residue. The chemical shift differences clearly extend beyond regions of structural difference, reflecting the extreme sensitivity of chemical shifts to very small structural or electronic changes within a protein.

It is not clear whether the observed structural differences between the wild-type and the mutant are sufficient to explain the 10-fold difference in their binding to thrombin. An additional factor to be considered is an alteration in the electrostatic surface properties of the protein in the vicinity of residue 47. Electrostatic calculations reveal that in the wild type there is a region of negative charge around the positively charged Lys-47 which originates from Asp-5 and Glu-8. In the mutant this alternation between positive and negative surface charge is replaced by a contiguous negatively charged patch formed by Asp-5, Glu-8, and Glu-47. We should also point out, however, that the reduction in binding affinity seems to be too small to be caused by the disruption of a specific electrostatic interaction involving Lys-47 and a negatively charged residue in the active site of thrombin (Dodt et al., 1984). This suggests that hydrophobic interactions in conjunction with general electrostatic complementarity may play a role in the interaction of thrombin with hirudin.

ACKNOWLEDGMENTS

We thank Dr. Ad Bax for useful discussions.

SUPPLEMENTARY MATERIAL AVAILABLE

One table giving the complete list of NOE interproton and hydrogen-bonding distance restraints and ϕ backbone and χ_1 side-chain torsion angle restraints used in the computation of the three-dimensional structure of recombinant wild-type hirudin and of the Lys-47 \rightarrow Glu mutant and seven figures showing additional NMR data, stereoviews, and atomic rms differences (43 pages). Ordering information is given on any current masthead page. The coordinates of the 32 SA structures and the restrained minimized mean structure (\overline{SA})_r for both the wild-type and mutant hirudin have been deposited in the Brookhaven Protein Data Bank.

Registry No. L-Lys, 56-87-1; L-Glu, 56-86-0; hirudin, 8001-27-2.

REFERENCES

- Aue, W. P., Bartholdi, E., & Ernst, R. R. (1976) *J. Chem. Phys.* **64**, 2229–2246.
- Bax, A. (1988) *Methods Enzymol.* (in press).
- Bax, A., Sklenar, V., Clore, G. M., & Gronenborn, A. M. (1987) *J. Am. Chem. Soc.* **109**, 6511–6513.
- Bergmann, C., Dodt, J., Köhler, S., Fink, E., & Gassen, H. G. (1986) *Biol. Chem. Hoppe-Seyler* **367**, 731–740.
- Billeter, M., Havel, T. F., & Wüthrich, K. (1987) *J. Comput. Chem.* **8**, 132–141.
- Braun, W., & Go, N. (1985) *J. Mol. Biol.* **186**, 611–626.
- Braunschweiler, L., & Ernst, R. R. (1983) *J. Magn. Reson.* **53**, 521–528.
- Brooks, B. R., Brucoleri, R. E., Olafson, B. D., States, D. J., Swamirathan, S., & Karplus, M. (1983) *J. Comput. Chem.* **4**, 187–217.
- Brünger, A. T., Clore, G. M., Gronenborn, A. M., & Karplus, M. (1986) *Proc. Natl. Acad. Sci. U.S.A.* **83**, 3801–3805.
- Brünger, A. T., Kuriyan, J., & Karplus, M. (1987a) *Science* **235**, 458–460.
- Brünger, A. T., Clore, G. M., Gronenborn, A. M., & Karplus, M. (1987b) *Protein Eng.* **1**, 399–406.
- Chan, S. J., Weiss, J., Konrad, M., White, T., Bahl, S.-D., Marks, D., & Steiner, F. (1981) *Proc. Natl. Acad. Sci. U.S.A.* **78**, 5401–5405.
- Chang, J.-Y. (1983) *FEBS Lett.* **164**, 307–313.
- Clore, G. M., Gronenborn, A. M., Brünger, A. T., & Karplus, M. (1985) *J. Mol. Biol.* **186**, 435–455.
- Clore, G. M., Brünger, A. T., Karplus, M., & Gronenborn, A. M. (1986a) *J. Mol. Biol.* **191**, 523–551.
- Clore, G. M., Nilges, M., Sukumaran, D. K., Brünger, A. T., Karplus, M., & Gronenborn, A. M. (1986b) *EMBO J.* **5**, 2729–2735.
- Clore, G. M., Sukumaran, D. K., Nilges, M., Zarbock, J., & Gronenborn, A. M. (1987a) *EMBO J.* **6**, 529–537.
- Clore, G. M., Gronenborn, A. M., Nilges, M., & Ryan, C. A. (1987b) *Biochemistry* **26**, 8012–8023.
- Crippen, G. M., & Havel, T. F. (1978) *Acta Crystallogr. A34*, 282–284.
- Davis, D. G., & Bax, A. (1985) *J. Am. Chem. Soc.* **107**, 2821–2822.
- Dodt, J., Schmitz, T., Schäfer, T., & Bergmann, C. (1986) *FEBS Lett.* **202**, 373–377.
- Dodt, J., Seemüller, U., & Fritz, H. (1987) *Biol. Chem. Hoppe-Seyler* **368**, 1447–1453.
- Dodt, J., Köhler, S., & Baici, A. (1988) *FEBS Lett.* **229**, 87–90.
- Driscoll, P. C., Gronenborn, A. M., Beress, L., & Clore, G. M. (1989) *Biochemistry* **28**, 2188–2198.
- Fenton, J. W., II (1981) *Ann. N.Y. Acad. Sci.* **370**, 468–495.
- Fenton, J. W., II, Landis, B. H., Walz, D. A., Bing, D. H., Feinmann, R. D., Zabinski, M. P., Sonder, S. A., Berliner, L. J., & Finlayson, J. S. (1979) in *The Chemistry and Physiology of Human Plasma Proteins* (Bing, D. H., Ed.) pp 151–183, Pergamon Press, New York.
- Fortkamp, E., Rieger, M., Heisterberg-Moutsers, G., Schweitzer, S., & Sommer, R. (1986) *DNA* **5**, 511–517.
- Griesinger, C., Sørensen, O. W., & Ernst, R. R. (1985) *J. Am. Chem. Soc.* **107**, 6394–6396.
- Griesinger, C., Sørensen, O. W., & Ernst, R. R. (1987) *J. Magn. Reson.* **75**, 474–492.
- Harvey, R. P., Degryse, E., Stefani, L., Schamber, F., Cazenave, J. P., Courtney, M., Tolstoshev, P., & Lecocq, J. P. (1986) *Proc. Natl. Acad. Sci. U.S.A.* **83**, 1084–1088.
- Havel, T. F. (1986) *DISGEO, QCPE No. 507*, Indiana University.
- Havel, T. F., & Wüthrich, K. (1985) *J. Mol. Biol.* **182**, 281–294.
- Havel, T. F., Kuntz, I. D., & Crippen, G. M. (1983) *Bull. Math. Biol.* **45**, 665–720.
- Haycraft, J. B. (1884) *Proc. R. Soc. London, Ser. B.* **36**, 478–487.

- Hyberts, S. G., Marki, W., & Wagner, G. (1987) *Eur. J. Biochem.* 164, 625-635.
- Ishikawa, A., Hafter, R., Seemuller, U., Gohel, J. M., & Graef, M. (1980) *Thromb. Res.* 19, 351-358.
- Jeener, J., Meier, B. H., Bachmann, P., & Ernst, R. R. (1979) *J. Chem. Phys.* 71, 4546-4533.
- Jones, T. A. (1978) *J. Appl. Crystallogr.* 11, 268-272.
- Kaptein, R., Zuiderweg, E. R. P., Scheek, R. M., Boelens, R., & van Gunsteren, W. F. (1985) *J. Mol. Biol.* 182, 179-182.
- Kloss, T., & Mittmann, U. (1982) *Langenbecks Arch. Chir.* 358, 548.
- Krstenansky, J. L., & Mao, S. J. T. (1987) *FEBS Lett.* 211, 10-16.
- Kuntz, I. D., Crippen, G. M., & Kollman, P. A. (1979) *Biopolymers* 18, 939-957.
- Macura, S., Huang, Y., Suter, D., & Ernst, R. R. (1981) *J. Magn. Reson.* 43, 259-281.
- Magnusson, S. (1972) *Enzymes (3rd Ed.)* 3, 277-321.
- Marion, D., & Wüthrich, K. (1983) *Biochem. Biophys. Res. Commun.* 113, 967-974.
- Marion, D., & Bax, A. (1988) *J. Magn. Reson.* (in press).
- Markwardt, F. (1970) *Methods Enzymol.* 19, 924-932.
- Markwardt, F. (1985) *Biomed. Biochim. Acta* 44, 1007-1013.
- Markwardt, F., Hauptmann, J., Nowak, G., Klessen, C., & Walsmann, P. (1982) *Thromb. Haemostasis* 47, 226-229.
- Markwardt, F., Fink, G., Kaiser, B., Klöcking, H.-P., Nowak, G., Richter, M., & Strürzebecher, J. (1988) *Pharmazie* 43, 202-207.
- Nilges, M., Clore, G. M., & Gronenborn, A. M. (1988a) *FEBS Lett.* 229, 317-324.
- Nilges, M., Gronenborn, A. M., Brünger, A. T., & Clore, G. M. (1988b) *Protein Eng.* 2, 27-38.
- Nilges, M., Clore, G. M., & Gronenborn, A. M. (1988c) *FEBS Lett.* 239, 129-136.
- Nowak, G., & Markwardt, F. (1980) *Exp. Pathol.* 18, 438-443.
- Owen, T. J., Krstenansky, J. L., Yates, M. T., & Mao, S. J. T. (1988) *J. Med. Chem.* 31, 1009-1011.
- Pardi, A., Billeter, M., & Wüthrich, K. (1984) *J. Mol. Biol.* 180, 741-751.
- Petersen, T. E., Roberts, H. R., Sottrup-Jensen, L., Magnusson, S., & Bagdy, D. (1976) in *Protides of Biological Fluids* (Peeters, H., Ed.) Vol. 23, pp 145-149, Pergamon Press, London and New York.
- Plateau, P., & Guéron, M. (1982) *J. Am. Chem. Soc.* 104, 7310-7311.
- Rance, M., Bodenhausen, G., Wagner, G., Wüthrich, K., & Ernst, R. R. (1985) *J. Magn. Reson.* 62, 497-500.
- Redfield, A. G., & Kuntz, S. D. (1975) *J. Magn. Reson.* 19, 250-254.
- Richardson, J. S. (1981) *Adv. Protein Chem.* 34, 167-339.
- Schechter, I., & Berger, A. (1967) *Biochem. Biophys. Res. Commun.* 27, 157-162.
- Stone, S. R., & Hofsteenge, J. (1986) *Biochemistry* 25, 4622-4628.
- Stone, S. R., Braun, P. J., & Hofsteenge, J. (1987) *Biochemistry* 26, 4617-4624.
- Sukumaran, D. K., Clore, G. M., Preuss, A., Zarbock, J., & Gronenborn, A. M. (1987) *Biochemistry* 26, 333-338.
- Wagner, G., Braun, W., Havel, T. F., Schaumann, T., Go, N., & Wüthrich, K. (1987) *J. Mol. Biol.* 196, 611-639.
- Walsmann, P., & Markwardt, F. (1981) *Pharmazie* 36, 653-660.
- Wüthrich, K. (1986) *NMR of Proteins and Nucleic Acids*, Wiley, New York.
- Wüthrich, K., Wider, G., Wagner, G., & Braun, W. (1982) *J. Mol. Biol.* 155, 311-319.
- Wüthrich, K., Billeter, M., & Braun, W. (1983) *J. Mol. Biol.* 169, 949-961.
- Zuiderweg, E. R. P., Boelens, R., & Kaptein, R. (1985) *Biopolymers* 24, 601-611.